

Coastal Synechococcus strains can exploit low oxygen habitats

Journal:	<i>Botany</i>
Manuscript ID	cjb-2024-0082.R1
Manuscript Type:	Research Article
Date Submitted by the Author:	n/a
Complete List of Authors:	Śliwińska-Wilczewska, Sylwia; Mount Allison University, Department of Biology; University of Gdansk, Institute of Oceanography Savoie, Mireille ; Mount Allison University, Department of Biology Campbell, Douglas ; Mount Allison University, Department of Biology
Is the manuscript for consideration in a Special Issue or Collection?:	UN Decade of Ocean Science for Sustainable Development
Keyword:	Colour, niches, OMZs, oxygen concentration, PC-rich strain, PE-rich strain, spectral wavebands, Synechococcus

SCHOLARONE™
Manuscripts

Coastal *Synechococcus* strains can exploit low oxygen habitats

Sylvia Śliwińska-Wilczewska^{1,2}, Mireille Savoie¹, and Douglas A. Campbell^{1,✉}

¹ Department of Biology, Mount Allison University, 53 York St., Sackville, NB, E4L 1C9, Canada

² Institute of Oceanography, University of Gdansk, 46 Pilsudskiego St, P81-378, Gdynia, Poland

✉ Correspondence: Douglas A. Campbell <dubhglascambeuil@gmail.com>

Abstract

We found that PhycoErythrin-rich *Synechococcus* achieved faster growth rates (μ), across the spectral bandwidths from 405 – 730 nm, under 2.5 μM $[\text{O}_2]$, characteristic of Oxygen Minimum Zones (OMZs), than under 250 μM $[\text{O}_2]$, whereas PhycoCyanin-rich strain showed generally similar μ under 2.5 and 250 μM $[\text{O}_2]$. For PhycoCyanin- and PhycoErythrin-rich *Synechococcus*, μ showed also positive linear responses to both Phycobiliproteins:Chlorophyll *a*, and to cumulative diel PSII electron flux, although the relations vary across strain and $[\text{O}_2]$. Electron transport downstream of Photosystem II was generally higher for both PhycoCyanin- and PhycoErythrin-rich strains under 250 μM $[\text{O}_2]$, since cyanobacteria show strong capacity for electron flow away from PSII to O_2 , particularly under excess excitation. **Even though electron transport was faster** under 250 μM $[\text{O}_2]$, the PhycoErythrin-rich strain showed a higher growth yield of electron transport under 2.5 μM $[\text{O}_2]$. PhycoErythrin-rich *Synechococcus* are currently typically found at greater depths, and lower light, than are PhycoCyanin-rich strains, but we suggest that the PhycoErythrin-rich strains are actually limited to lower light by an interaction

between light and full air-saturated [O₂]. In expanding Oxygen Minimum Zones PhycoErythrin-rich strains will likely exploit higher light niches, across a wider spectral range.

Key words: Colour, niches, OMZs, oxygen concentration, PC-rich strain, PE-rich strain, spectral wavebands, *Synechococcus*

Introduction

Since the mid-20th century, declining oxygen concentrations in regions of the open ocean, and in coastal waters (Breitburg et al. 2018) are affecting productivity, biodiversity, and biogeochemical cycles in marine ecosystems (Keeling et al. 2010). Low oxygen environments in the ocean, termed Oxygen Minimum Zones (OMZ) have expanded to an area equivalent to the European Union, and the global volume of oxygen-free water has quadrupled (Breitburg et al. 2018). It is thus necessary to understand which species will survive and dominate under ongoing and predicted changes in ocean and coastal oxygen concentrations.

Oxygenic picocyanobacteria numerically dominate the phytoplankton across vast tracts of the world's oceans, notably in oligotrophic regions, but also in some coastal ecosystems (Larsson et al. 2014; Śliwińska-Wilczewska et al. 2018a; Aguilera et al. 2023). Oxygen is a product of photosynthesis, and a substrate for reductant consumption, but also has potential to damage Photosystem II (PSII) protein subunits (Andersson et al. 1992). The oxygen evolving complex of PSII can also be directly inactivated by a photon in the UV or blue range directly absorbed by the Mn₄Ca cluster (Hakala et al. 2005; Partensky et al. 2018); therefore, oxygen interacts with spectral band to influence the balance between productive photosynthesis and costly photoinactivations (Murphy et al. 2017). OMZ pose challenges for aerobic organisms (Breitburg et al. 2018), but

picocyanobacteria inhabiting OMZs have genetic adaptations enabling them to tolerate and even thrive in oxygen-depleted environments, such as changes in energy metabolism, antioxidant defense mechanisms, and cellular structures optimized for oxygen scavenging and storage (Ulloa et al. 2012, 2021; Bagby and Chisholm 2015; Partensky et al. 2018; Callieri et al. 2022; Wong et al. 2023).

Picocyanobacteria also show photosynthetic adaptations to spectral wavebands, ranging from short-wavelength blue light (Luimstra et al. 2018), through green and yellow light to long-wavelength red light. Plankton ecologists have long acknowledged that a diverse array of photosynthetic pigments allows cyanobacteria species to exploit different spectral wavebands (Falkowski et al. 2004; Stomp et al. 2007). The ecological success of picoplanktonic *Synechococcus* strains throughout the photic oceanic water column (Flombaum et al. 2013) results in part from diverse strategies to respond to variations in their environment (Scanlan 2012; Doré et al. 2020). The genus *Synechococcus* is genetically diverse and divided into several major clusters. Picocyanobacteria from *Synechococcus* cluster 5, often found in marine, brackish and freshwater environments (Sánchez-Baracaldo et al. 2019; Aguilera et al. 2023), includes sub-clusters of strains rich in phycoerythrin (PE-rich), which imparts a range of orange, reddish, pink, and purple colors, as well as sub-clusters of strains rich in phycocyanin (PC-rich), which color the organism in various shades of blue-green (Stomp et al. 2004). Competition experiments demonstrate that PC-rich and PE-rich strains can coexist in white light but show spectral niche differentiation (Haverkamp 2008; Callieri et al. 2012).

PE-rich strains, with high content of the chromophore phycourobilin (PUB), dominate oligotrophic deep waters where blue light predominates, and deep communities in more mesotrophic marine waters, characterized by blue-green light environments (Stomp et al. 2004;

Haverkamp et al. 2009) are shifting towards PE-rich *Synechococcus* with more phycoerythrobilin (PEB). Conversely, PC-rich strains prevail near the surface, and in turbid waters where orange and red light dominate. The widespread coexistence of PC-rich and PE-rich picocyanobacteria is observed in waters of intermediate turbidity, such as mesotrophic lakes and coastal seas (Haverkamp 2008; Haverkamp et al. 2009).

Our aim was to test the growth and functional responses of PC-rich and PE-rich *Synechococcus* cultures to the interaction of different oxygen concentrations (250 μM or 2.5 μM $[\text{O}_2]$), and spectral wavebands (405 – 730 nm). We thus empirically answer the question posed by Wong et al. (2023) regarding the sensitivity of modern picocyanobacteria to low levels of O_2 and a wide range of wavebands found across depths and trophic levels.

Materials and methods

Culture condition and experimental setup

Xenic cultures of PC-rich (CCBA_077) and PE-rich (CCBA_127) *Synechococcus* were obtained from the Culture Collection of Baltic Algae (<https://ccba.ug.edu.pl/pages/en/home.php>) (Latala et al. 2006). *Synechococcus* strains were cultured in Tissue Culture Flasks (VWR International, Cat. No. 10062-872, PA, USA) and transferred biweekly to fresh f/2 media (Guillard 1975) prepared at a salinity of 8 PSU, reflective of their natural brackish habitat. Pre-cultures were maintained in incubators with full air saturated dissolved oxygen concentration $[\text{O}_2]$ of 250 μM , 22°C, with a light/dark cycle of 12 hours (h) and Photosynthetically Active Radiation (PAR) of 10 $\mu\text{mol photons m}^{-2}\text{s}^{-1}$ from Philips Cool White F14T5/841 Alto, 14 watts, fluorescent bulbs.

Controlled growth experiments were performed using MCMIX-OD PSI Multicultivators (Photon Systems Instruments, Drásov, Czech Republic) set to 22°C. Each of 8 round bottom

cylindrical glass tubes contained 75 mL of f/2 medium and 5 mL of growing pre-culture. These parameters allowed for exponential growth of the cultures from the beginning of the experiment, with little lag phase. Inoculation of culture tubes took place in the afternoon, with a period of low light and then 12 h darkness before a sinusoidal 12 h photoperiod cycle commenced at 07:00 the following morning, with peak PAR of $180 \mu\text{mol photons m}^{-2}\text{s}^{-1}$ reached at 13:00 each day.

Each tube was maintained under an individual combination of one of 7 spectral wavebands centred at 405, 450, 470, 530, 620, 660, or 730 nm and under 250 μM or 2.5 μM $[\text{O}_2]$. Culture tubes were closed with an inert silicone stopper perforated by an aeration input tube extending to the bottom of the culture tube, and a pressure outlet tube. We used aeration with a total gas flow rate of around $\sim 140 \text{ mL min}^{-1} \text{ tube}^{-1}$ through a $0.2 \mu\text{m}$ sterile microfilter provided via a G400 gas mixing system (Qubit Systems Inc., Kingston, Ontario, Canada). $\sim 250 \mu\text{M}$ $[\text{O}_2]$ was achieved by sparging with lab air (78% N_2 , 21% O_2 , 1% Ar and 0.05% CO_2). $\sim 2.5 \mu\text{M}$ $[\text{O}_2]$ was achieved by sparging with a gas mixture containing 99.95% N_2 and 0.05% CO_2 . $[\text{O}_2]$ *in situ* was verified using oxygen optodes (PyroScience, Germany) inserted into tubes for real-time measurements (data not presented), with software correction to account for the salinity of the media (8 PSU). The pH of tested cultures remained about 8, with limited fluctuation during the growth experiment (data not presented).

Chlorophyll-specific growth rates

Picocyanobacterial growth was monitored every 5 minutes by automatically recording OD_{680} , OD_{720} , and ΔOD ($\Delta\text{OD} = \text{OD}_{680} - \text{OD}_{720}$) for at least 5 days, independently for each culture tube. The chlorophyll-specific growth rates (μ) were determined by fitting logistic growth curves using a modified Levenberg-Marquardt fitting algorithm (Elzhov et al. 2023) to plots of the

chlorophyll *a* proxy of ΔOD vs. elapsed time (d) for each combination of strain, spectral waveband, and $[O_2]$.

Picocyanobacteria cell counts

Picocyanobacterial cells mL^{-1} were estimated using linear regression models of OD at 680 nm or 720 nm vs. calibration counts of cell suspension densities (cell mL^{-1}) (Table S1). The OD of cultures was measured using MCMIX-OD PSI Multicultivators (Photon Systems Instruments, Drásov, Czech Republic) and cell suspension density measures were conducted using an ImageXpress Pico Digital microscope equipped with CMOS camera and LED+ image autofocus (ImageXpress Pico Automated Cell Imaging System, Molecular Devices, LLC., CA, USA). Culture samples were preserved with 4% glutaraldehyde and kept at $-80^{\circ}C$ until the microscopy measures. Fixed samples of culture ($V = 10 \mu L$) were transferred to surface treated Tissue Culture (TC) black walled 96-well plates (Corning® Falcon® Microplate, MilliporeSigma, Merck, Darmstadt, Germany) with a transparent flat bottom containing $200 \mu L$ of f/2 media and centrifuged using a Beckman J-20 centrifuge with a swinging bucket JS-4.3 rotor at 4500 rpm (Beckman Coulter, Brea, California, United States). Cells were imaged with the Cy5 channels (Excitation: 630/40 nm; Emission: 695/45 nm; Dichroic: 655 nm) using selectable confocal geometries, which differentiates cyanobacterial cells from co-occurring heterotrophic bacteria, and counted using a 63x objective in fluorescence imaging modes. Quantitative analysis on images acquired from automated microscopy obtained from 96-well microplates was performed using the CellReporterXpress Image Acquisition and Analysis Software. The representative cell number mL^{-1} was calculated based on the dilution factor and selected count area from each well (Wlodkowic et al. 2022).

Pigment content and pigment ratio

Whole-cell absorbance spectra of picocyanobacteria cells were collected using an integrating cavity spectrophotometer (CLARITY 17 UV/Vis/NIR, On-Line Instrument Systems, Inc., Bogart, GA, USA) according to the method proposed by Blake and Griff (2012). The sample and reference observation cavities of the spectrophotometer were filled with 8 mL of f/2 medium at salinity 8 PSU. After establishing a baseline absorbance spectra from 375 to 710 nm, 4 mL culture medium was replaced with 4 mL of culture in the sample cavity. Pathlength corrected absorbance per cm was calculated using Javorfi coefficients (Javorfi et al. 2006). We then conducted estimations of pigment content ($\mu\text{g mL}^{-1}$) including Chlorophyll *a* (Chl *a*), Carotenoids (Car), Phycoerythrin (PE), Phycocyanin (PC), and Allophycocyanin (APC) from the PC-rich and PE-rich *Synechococcus* cultures. These estimations were based on established linear correlations between pigment content, determined through extraction methods (Strickland and Parsons 1972; Bennett and Bogorad 1973), and absorbance values of individual pigment peaks (Car; 480 nm, PE; 565 nm, PC; 620 nm, APC; 650 nm, and Chl *a*; 665 nm) obtained from whole-cell absorbance spectra (Table S2). Additionally, we summed PE, PC, and APC protein to total Phycobiliproteins content.

Using whole-cell absorbance spectra of *Synechococcus* cultures, we also estimated Photosynthetically Usable Radiation (PUR; $\mu\text{mol photons m}^{-2}\text{s}^{-1}$) according to (Morel 1978).

PSII effective absorption cross section of PSII, turnover time of PSII photochemistry, and photochemical quenching

We harvested 4 mL of picocyanobacteria cultures repeatedly across the growth trajectories for photophysiological characterizations. For the low oxygen cultures, to ensure

photophysiological measurements were taken at low O_2 of $\sim 2.5 \mu M$, we bubbled gently with N_2 from a gas cylinder during measurements. $[O_2]$ was verified in culture samples for photophysiological measurements using oxygen optodes (PyroScience, Germany) inserted (data not presented).

We used Fast Repetition & Relaxation chlorophyll fluorescence (FRRf) (Kolber et al. 1998) (Solisense, USA), with a lab built temperature control jacket ($22^\circ C$), to apply a series of 100 excitation flashlets of $1.6 \mu s$ to drive saturation of PSII variable fluorescence, followed immediately by logarithmically spaced flashlets to track relaxation of variable fluorescence. Induction/relaxation trajectories were fit using the onboard Solisense LIFT software (Falkowski and Kolber 1993; Kolber et al. 1998).

We used a double tap protocol (Xu et al. 2017), where FRRf induction/relaxation trajectories were collected during a rapid actinic light curve sequence increasing in steps of 10 s at 0, 20, 40, 80, 160, and $320 \mu mol \text{ photons } m^{-2}s^{-1}$ PAR. We applied 1 s darkness between the sequential 10 s steps of the light response curves, to allow re-opening of PSII immediately after application of the sequential increasing light steps. Flashlets and actinic light were delivered from LED emitters centred at Ex_{445nm} , preferentially exciting chlorophyll; Ex_{470nm} , preferentially exciting phycourobilin (PUB); Ex_{535nm} , preferentially exciting phycoerythrin (PE); or Ex_{590nm} , preferentially exciting phycocyanin (PC). Excitation flashlets and actinic light wavebands were matched for each run. These actinic and excitation wavebands in turn approximated 4 of our 7 growth light wavebands (450, 470, 530 & 620 nm), allowing us to evaluate *in situ* photosynthetic performance for those culture conditions.

Flashlet power delivered to the samples during the $1.6 \mu s$ flashlet duration was adjusted to achieve saturation of variable fluorescence; Ex_{445nm} at $60000 \mu mol \text{ photons } m^{-2}s^{-1}$ PAR; Ex_{470nm}

at 30000 $\mu\text{mol photons m}^{-2}\text{s}^{-1}$ PAR; $\text{Ex}_{535\text{nm}}$ at 25000 $\mu\text{mol photons m}^{-2}\text{s}^{-1}$ PAR; while for $\text{Ex}_{590\text{nm}}$ excitation power at 14000 $\mu\text{mol photons m}^{-2}\text{s}^{-1}$, calibrated using a quantum sensor (LI-250, LI-COR, Inc.) in the temperature controlled cuvette.

We estimated effective absorption cross section of PSII (σ_{PSII} ; $\text{nm}^2 \text{ quanta}^{-1}$); turnover time of PSII photochemistry (τ_{PSII} ; μs); and the photochemical quenching coefficient (q_p) using the FRRf induction curves, following (Xu et al. 2017). We fit a model with three τ_{PSII} to describe the re-opening of PSII after closure by the saturating flash train. For subsequent analyses we estimated an average of the three τ_{PSII} , weighted by their respective amplitudes, to describe the overall time to reopen PSII after closure.

PSII electron flux

We calculated (Eq. (1)) an uncalibrated fluorescence based estimator for volumetric electron transport, JV_{PSII} , ($\text{k} \times \text{e}^- \text{ L}^{-1} \text{ s}^{-1}$) under $\text{Ex}_{445\text{nm}}$, blue; $\text{Ex}_{470\text{nm}}$, blue-green; $\text{Ex}_{535\text{nm}}$, green; or $\text{Ex}_{590\text{nm}}$, red-orange excitation bands (Oxborough et al. 2012; Boatman et al. 2019; Tortell and Suggett 2021).

$$JV_{\text{PSII}} = \frac{\sigma_{\text{PSII}}' \times q_p \times I \times F_O}{\sigma_{\text{PSII}}} \quad (1)$$

where σ_{PSII}' is effective absorption cross section for PSII photochemistry under the relevant actinic PAR step ($\text{nm}^2 \text{ quanta}^{-1}$); q_p is an estimate of the fraction of PSII open for photochemistry estimated according to Oxborough and Baker (1997); I is the applied PAR ($\mu\text{mol photons m}^{-2}\text{s}^{-1}$); F_O is the minimum fluorescence from a given sample and excitation waveband (relative fluorescence) and σ_{PSII} is the maximum effective absorption cross section for PSII photochemistry from a given sample and excitation waveband ($\text{nm}^2 \text{ quanta}^{-1}$).

We calibrated the JV_{PSII} estimator to absolute rates of electron transport (Eq. (2)) using parallel measures of oxygen evolution ($\mu\text{mol O}_2 \text{ L}^{-1} \text{ s}^{-1}$), captured simultaneously with the FRRf measures, taken below light saturation of electron transport to limit distortion from electron fluxes back to oxygen under super-saturating light (Hughes et al. 2018), using a FireSting robust oxygen probe (PyroScience, Germany) inserted in the cuvette for select Rapid Light Curve (RLC) runs (Table S3).

$$JV_{PSII}(e^- \text{ L}^{-1} \text{ s}^{-1}) = \frac{\text{Uncalibrated } JV_{PSII}(e^- \text{ L}^{-1} \text{ s}^{-1})}{\text{Calibration slope}} \quad (2)$$

We converted JV_{PSII} ($\mu\text{mol e}^- \text{ L}^{-1} \text{ s}^{-1}$) to JV_{PSII} ($\mu\text{mol e}^- \mu\text{mol Chl } a^{-1} \text{ d}^{-1}$) by performing Chl a ($\mu\text{g L}^{-1}$) measurements using Trilogy Laboratory Fluorometer (Turner Designs, Inc., CA, USA) equipped with Chlorophyll In-Vivo Module, on the samples taken for the FRRf measurements.

To generate an index of the ratio of Chl a : PSII we divided PSII electron transport ($e^- \text{ PSII}^{-1} \text{ s}^{-1}$) by JV_{PSII} ($e^- \text{ Chl}^{-1} \text{ s}^{-1}$), both estimated under $\text{Ex}_{445\text{nm}}$, with units cancelling to Chl a : PSII. Since the number of Chl a directly associated with the core of PSII is fixed, variations in Chl a to PSII reflect changes in the PSI:PSII ratio, and possibly the presence of other chl-containing complexes.

Statistical analysis

We used R version 4.3.0 (R Core Team 2023) running under RStudio (Posit team 2022). We performed three-way factorial ANOVA (*aov()* function; R Base package) to determine whether strain, growth waveband, and $[\text{O}_2]$ significantly influence the chlorophyll-specific growth rate ($\mu; \text{d}^{-1}$; Table S4) or pigment content (Table S5). We also performed three-way factorial ANOVA (*aov()* function) to determine whether strain, Actinic PAR, and $[\text{O}_2]$ significantly influence the

responses of σ_{PSII} (Table S6); τ_{PSII} (Table S7); q_p (Table S8); or JV_{PSII} (Table S9) to increasing light. We fit the light response curves of JV_{PSII} with a three parameter model (Harrison and Platt 1986) using (Elzhov et al. 2023) for *nlsLM()* function. Three-way factorial ANOVA (*aov()* function; R Base package) was performed to determine whether strain, growth waveband, and $[\text{O}_2]$ significantly influence Chl *a* to PSII (Table S10).

We used *t*-tests of linear regressions to compare data across different strains and $[\text{O}_2]$ for a given growth waveband, for chlorophyll-specific growth rate vs. Phycobiliproteins to Chl *a* ratio (Table S11). We also performed *t*-tests of linear fits to compare data across different strains and $[\text{O}_2]$ in situations in which cultures were excited by, and growing in, corresponding growth wavebands of 450, 470, 530, or 620 nm, for chlorophyll-specific growth rate vs. JV_{PSII} (Table S12). Statistical differences for all analyses were determined at significance level $\alpha = 0.05$.

The manuscript was prepared as a Rmarkdown document (Handel 2020) with figures plotted using ggplot2 (Wickham 2016) and patchwork (Pedersen 2024) packages. All metadata, data, and code is available on GitHub (<https://github.com/FundyPhytoPhys/BalticO2>).

Results

Chlorophyll-specific growth rates across $[\text{O}_2]$, spectral wavebands, and strains

We used logistic curve fits (Fig. S1) to determine chlorophyll-specific growth rates (μ ; d^{-1}) for PC-rich and PE-rich cultures of *Synechococcus* grown under spectral wavebands centred at 405, 450, 470, 530, 620, 660, or 730 nm, and $[\text{O}_2]$ of 250 μM or 2.5 μM (Fig. 1). Growth curves, tracked as OD_{680} , OD_{720} , ΔOD and logistic fits of ΔOD vs. elapsed time are shown in Fig. S1 in Supplementary materials. Cell-specific growth rates (μ) were also determined using OD_{720} (Fig. S2). Strain, growth waveband, $[\text{O}_2]$, and their interactions, significantly affected μ (Table S4).

PC-rich and PE-rich *Synechococcus* grow under 2.5 μM $[\text{O}_2]$, across the range of tested spectral wavebands from 405 – 730 nm. In contrast, under 250 μM $[\text{O}_2]$, the PC-rich strain failed to grow under 405 nm, while the PE-rich strain failed to grow under 405, 450, and 730 nm. The PC-rich strain showed generally similar growth rates under 2.5 and 250 μM $[\text{O}_2]$, across tested spectral wavebands (nm). In contrast the PE-rich strain achieved faster growth rates under 2.5 μM $[\text{O}_2]$ than under 250 μM $[\text{O}_2]$.

PC-rich *Synechococcus* showed a peak in growth rate under both $[\text{O}_2]$ and red light of 620 or 660 nm, absorbed by phycocyanin and chlorophyll. Under 2.5 μM $[\text{O}_2]$ the PE-rich strain showed high growth rates under 530 nm – 660 nm absorbed by phycoerythrin, phycocyanin, and chlorophyll; while under 250 μM $[\text{O}_2]$, the PE-rich strain showed the highest growth rate under green light of 530 nm absorbed by phycoerythrin.

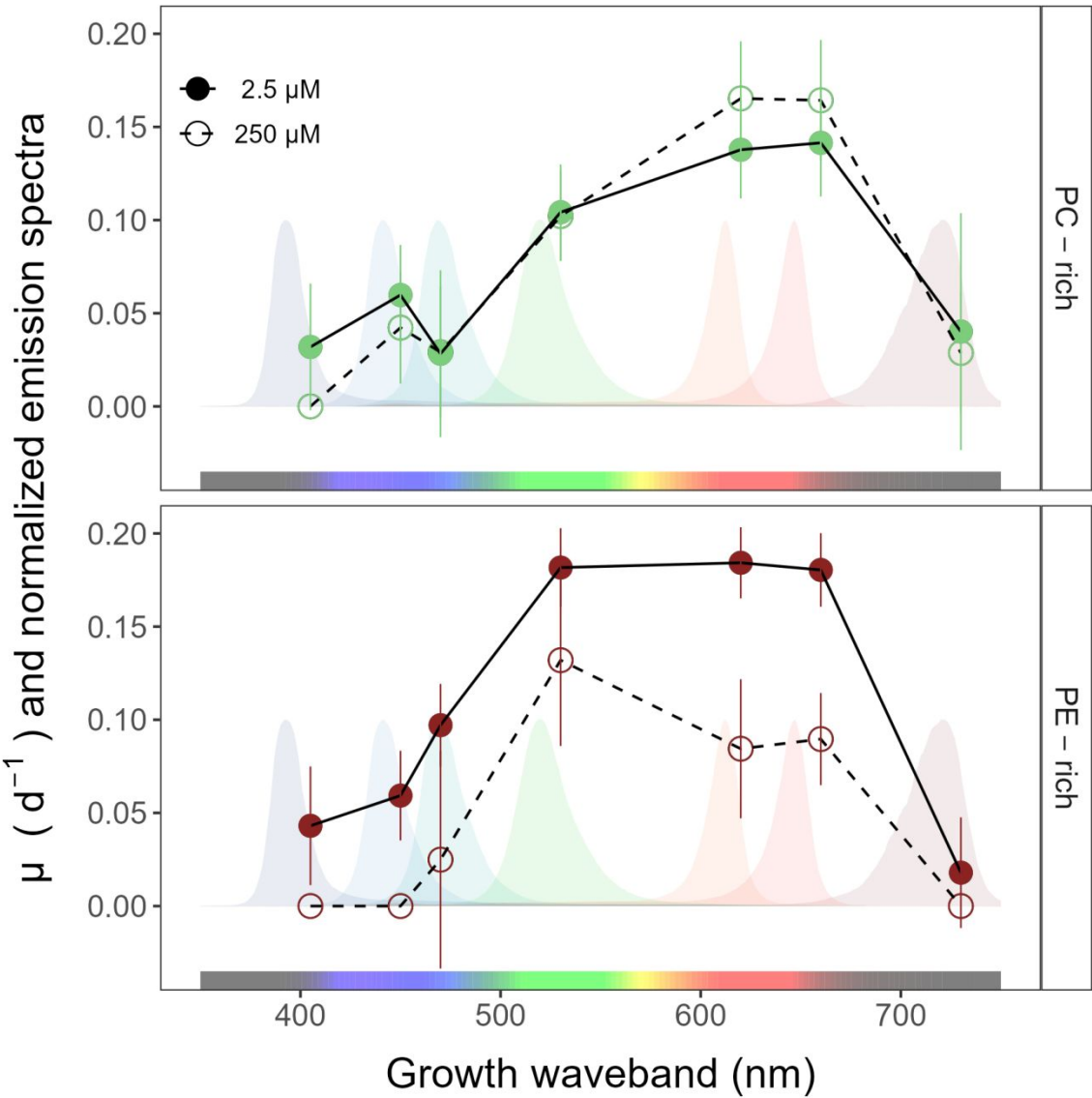


Fig. 1: Chlorophyll-specific growth rates (μ ; d^{-1}) vs. growth waveband (nm, shaded regions). Growth rates (\pm SE) were estimated from logistic fits of chlorophyll proxy $\text{OD}_{680} - \text{OD}_{720}$ (ΔOD) vs. elapsed time (Fig. S1), for PC-rich (green circle) and PE-rich (red circle) cultures of *Synechococcus* grown at spectral wavebands of 405, 450, 470, 530, 620, 660, or 730 nm, and $[\text{O}_2]$ of 250 μM (open symbols and dashed line) or 2.5 μM (closed symbols and solid line).

Pigment content and pigment ratio across [O₂], spectral wavebands, and strains

Fig. 2a presents Chlorophyll *a* (Chl *a*), Phycobiliproteins (Phyco), or Carotenoids (Car) content (pg cell⁻¹) vs. growth waveband (nm) for PC-rich and PE-rich cultures of *Synechococcus* grown at spectral wavebands centred at 405, 450, 470, 530, 620, 660, or 730 nm and 250 or 2.5 μM [O₂]. We also calculated the Car to Chl *a* ratio, and the ratio of the sum of Phycobiliproteins to Chl *a* (μg:μg) for each strain (Fig. S3). Moreover, phycobiliproteins:Chlorophyll *a* ratio (μg:μg) and chlorophyll-specific growth rates (μ; d⁻¹) vs. Photosynthetically Usable Radiation (PUR, μmol photons m⁻²s⁻¹) for PC-rich and PE-rich cultures of *Synechococcus* grown at spectral wavebands of 405, 450, 470, 530, 620, 660, or 730 nm and 250 μM [O₂] or 2.5 μM [O₂] are presented in Fig. S4.

To focus on the responses of growing cells, we omit pigmentation data from those PE-rich cultures which showed negligible growth under 405, 450, 730 nm and 250 μM [O₂]; and from those PC-rich cultures which showed negligible growth under 405 nm and 250 μM [O₂].

Strain, growth waveband, [O₂], and their interactions, significantly affected cell-specific Chl *a*, Phycobiliproteins, and Car content (Table S5). For the PC-rich strain, the highest Chl *a*, Phycobiliproteins, and Car contents were recorded after growth under 730 nm. The phycobiliproteins content was higher under 250 μM [O₂] than under 2.5 μM [O₂] for the PC-rich strain. In contrast, for PE-rich *Synechococcus*, phycobiliproteins content was significantly lower under 250 μM [O₂] than under 2.5 μM [O₂], with the highest phycobiliproteins content under 620 nm and 2.5 μM [O₂].

Chlorophyll-specific growth rates (μ; d⁻¹) show positive linear responses to the Phycobiliproteins:Chlorophyll *a* ratio (μg:μg), for both PC-rich and PE-rich *Synechococcus* (Fig. 2b), although the relations vary across strain and [O₂] (Table S11).

293

Draft

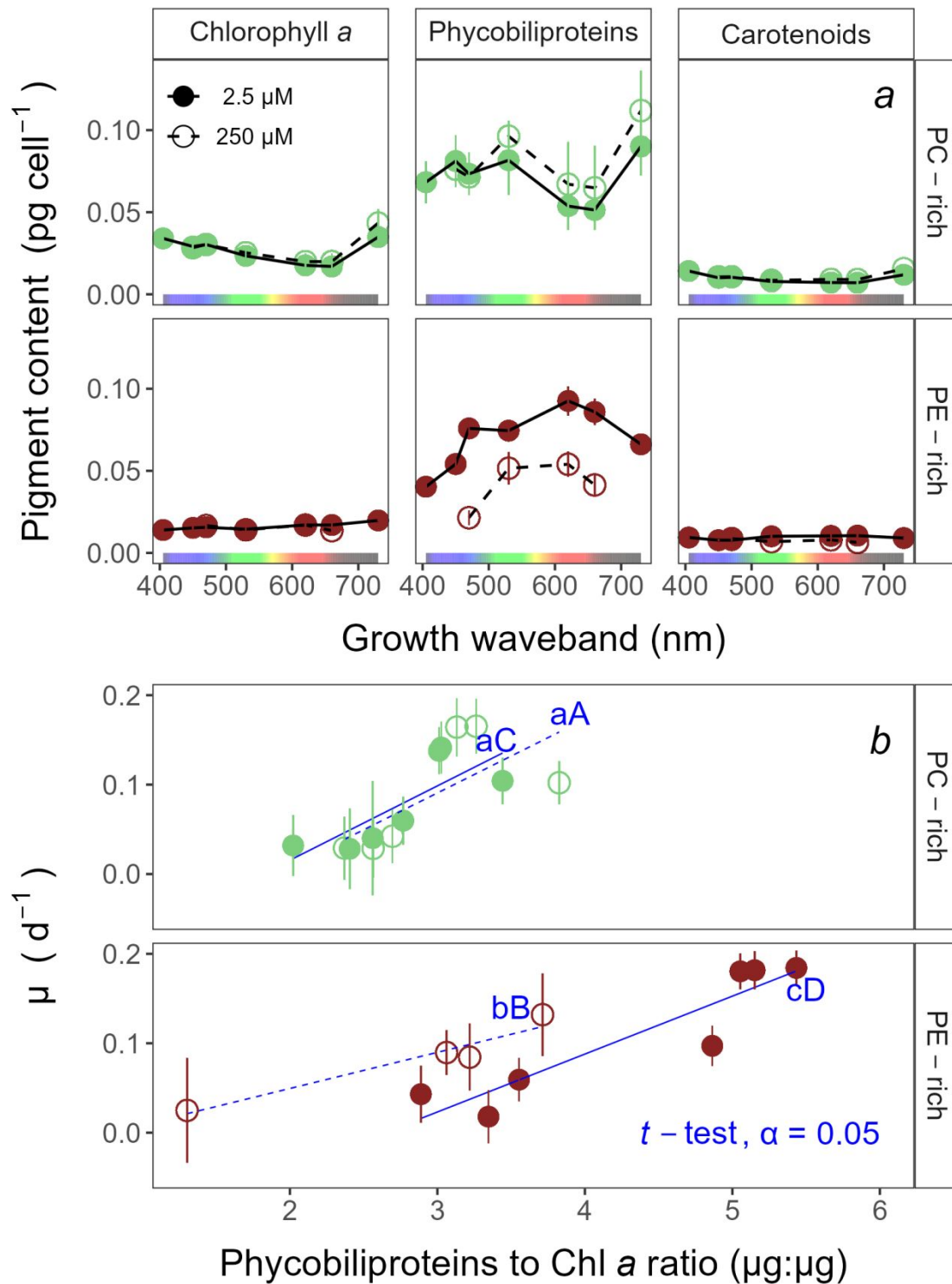


Fig. 2: Pigment content (pg cell⁻¹) vs. growth waveband (nm) (a) and Chlorophyll-specific growth rates (μ ; d⁻¹) vs. Phycobiliproteins:Chlorophyll *a* ratio (μ g: μ g) (b) for PC-rich (green circle) and

PE-rich (red circle) cultures of *Synechococcus* grown at spectral wavebands of 405, 450, 470, 530, 620, 660, or 730 nm and 250 μM $[\text{O}_2]$ (open symbols and dashed line) or 2.5 μM $[\text{O}_2]$ (closed symbols and solid line). Data not presented for those PE-rich cultures which showed negligible growth under 405, 450, 730 nm and 250 μM $[\text{O}_2]$; nor for those PC-rich cultures which showed negligible growth under 405 nm and 250 μM $[\text{O}_2]$. Blue lines show linear model fit for data from each strain and $[\text{O}_2]$ (solid for 2.5 μM $[\text{O}_2]$ or dashed for 250 μM $[\text{O}_2]$) across spectral wavebands. Different blue lowercase letters indicate statistically significant differences between the fit models for different $[\text{O}_2]$ within a given strain. Different blue uppercase letters indicate statistically significant differences between the fit models for different strains within a given $[\text{O}_2]$ (t -test; $p < 0.05$).

Effective absorption cross sections, turnover times, and photochemical quenching of PSII across $[\text{O}_2]$, spectral wavebands, and strains

Light response curves of effective absorption cross section of PSII (σ_{PSII} ; $\text{nm}^2 \text{ quanta}^{-1}$); turnover time of PSII photochemistry (τ_{PSII} ; μs); and the photochemical quenching coefficient (q_p) vs. Actinic PAR ($\mu\text{mol photons m}^{-2}\text{s}^{-1}$) (Fig. 3a-c) are shown for PC-rich and PE-rich cultures grown in, and excited by, corresponding wavebands of 450, 470, 530, or 620 nm, at 250 μM or 2.5 μM $[\text{O}_2]$. We omit functional data determined for those PE-rich cultures which showed negligible growth under 405, 450, 730 nm and 250 μM O_2 ; and for those PC-rich cultures which showed negligible growth under 405 nm and 250 μM O_2 . In the Supplementary materials (Fig S5-S7), we also show the light response curves for all available excitation ($\text{Ex}_{445\text{nm}}$, blue; $\text{Ex}_{470\text{nm}}$, blue-green; $\text{Ex}_{535\text{nm}}$, green; or $\text{Ex}_{590\text{nm}}$, orange) and growth waveband (450, 470, 530, or 620 nm) cross-combinations.

σ_{PSII} (Fig. 3a), a measure of excitation driving PSII photochemistry, was low and shows little change with increasing actinic light during excitation through chlorophyll at $\text{Ex}_{445\text{nm}}$. For the PC-rich strain, under orange excitation at $\text{Ex}_{590\text{nm}}$, σ_{PSII} showed an initial small increase from darkness to the growth light level, followed by a mild decrease with increasing Actinic PAR, and was higher at $250 \mu\text{M} [\text{O}_2]$ compared to $2.5 \mu\text{M} [\text{O}_2]$. For the PE-rich strain, we again see a small increase from darkness to the growth light level, followed by a decrease in σ_{PSII} with increasing Actinic PAR. Moreover, for the PE-rich strain σ_{PSII} was higher in low $[\text{O}_2]$ conditions than in high $[\text{O}_2]$ conditions. Strain, Actinic PAR, and $[\text{O}_2]$ significantly influenced σ_{PSII} under excitation at $\text{Ex}_{590\text{nm}}$ (Table S6).

For the PC-rich strain, across the excitation wavebands tested, τ_{PSII} showed an acceleration (decrease) from darkness to growth light Actinic PAR (Fig. 3b), to a plateau of $\sim 800 \mu\text{s}$. PE-rich strains, on the other hand, showed a progressive acceleration (decrease) with increasing Actinic PAR under excitation at $\text{Ex}_{470\text{nm}}$, $\text{Ex}_{535\text{nm}}$, or $\text{Ex}_{590\text{nm}}$, declining towards $\sim 400 \mu\text{s}$ under $\text{Ex}_{590\text{nm}}$. Thus, the PE-rich strain showed more capacity to remove electrons from PSII. τ_{PSII} was generally faster (smaller) for both PC-rich and PE-rich strains under $250 \mu\text{M} [\text{O}_2]$. Strain, Actinic PAR, and $[\text{O}_2]$ significantly affected τ_{PSII} at $\text{Ex}_{470\text{nm}}$, $\text{Ex}_{535\text{nm}}$ and $\text{Ex}_{590\text{nm}}$ (Table S7).

q_p , a measure of the fraction of PSII available for photochemistry, showed a strong decrease with increasing Actinic PAR across the excitation wavebands tested (Fig. 3c). q_p generally remained higher for both PC-rich and PE-rich strains under $250 \mu\text{M} [\text{O}_2]$. Strain, Actinic PAR, and $[\text{O}_2]$ significantly affected q_p at $\text{Ex}_{470\text{nm}}$, $\text{Ex}_{535\text{nm}}$, and $\text{Ex}_{590\text{nm}}$ (Table S8).

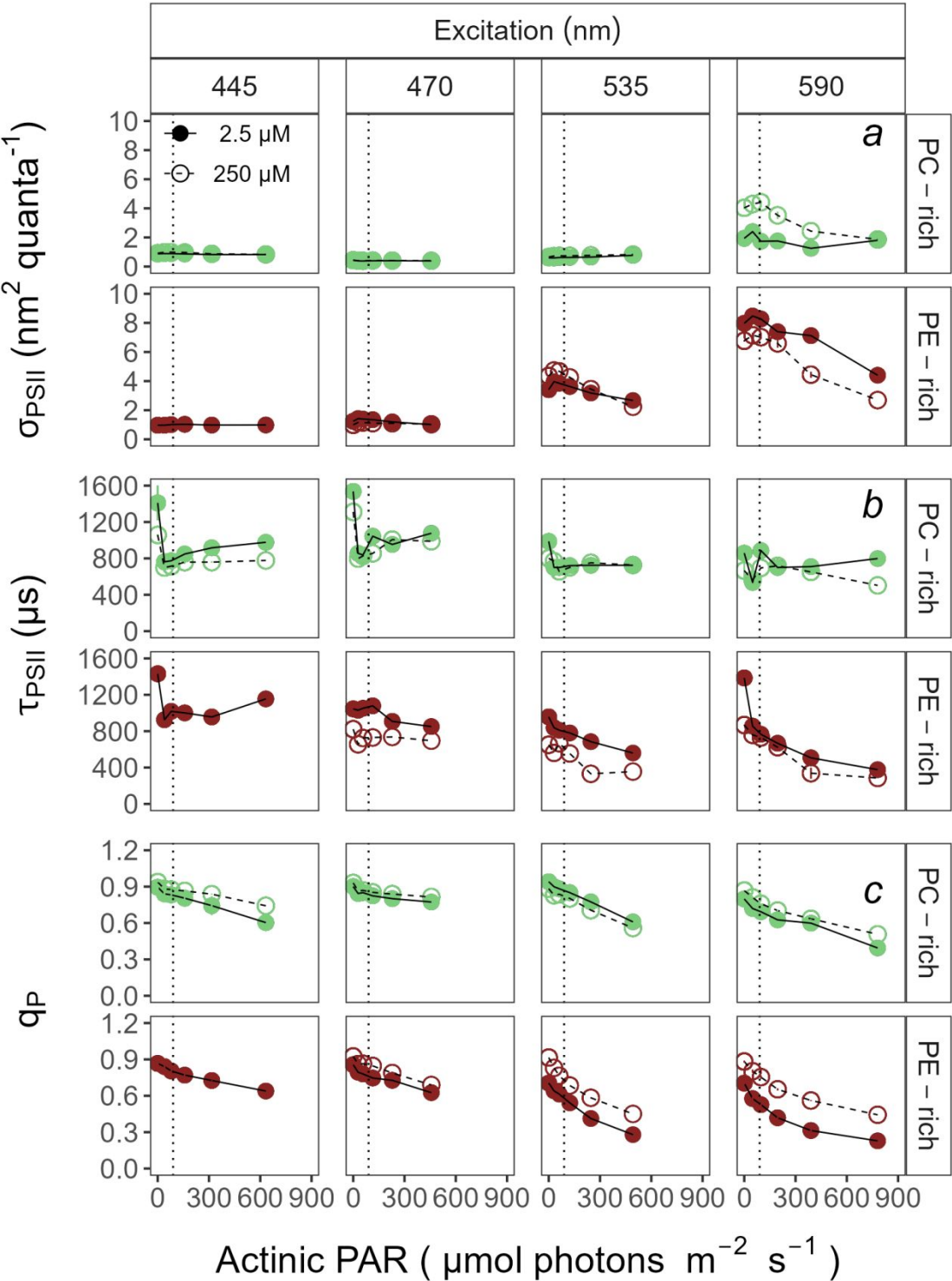


Fig. 3: Effective absorption cross section of PSII (σ_{PSII} ; nm² quanta⁻¹) (a); turnover time of PSII photochemistry (τ_{PSII} ; μs) (b); or photochemical quenching coefficient (q_P) (c) vs. Actinic PAR

($\mu\text{mol photons m}^{-2}\text{s}^{-1}$). Parameters were estimated using FRRf induction curves with excitation (columns) at $\text{Ex}_{445\text{nm}}$, blue; $\text{Ex}_{470\text{nm}}$, blue-green; $\text{Ex}_{535\text{nm}}$, green; or $\text{Ex}_{590\text{nm}}$, orange; for PC-rich (green circle) or PE-rich (red circle) cultures of *Synechococcus*. Data show situations in which cultures were excited by, and growing in, corresponding growth wavebands of 450, 470, 530, or 620 nm and 250 μM $[\text{O}_2]$ (open symbols and dashed line) or 2.5 μM $[\text{O}_2]$ (closed symbols and solid line). The vertical lines show half diel peak PAR growth light of 90 $\mu\text{mol photons m}^{-2}\text{s}^{-1}$. Data not presented for those PE-rich cultures which showed negligible growth under 405, 450, 730 nm and 250 μM $[\text{O}_2]$; nor for those PC-rich cultures which showed negligible growth under 405 nm and 250 μM $[\text{O}_2]$.

PSII electron flux across $[\text{O}_2]$, spectral wavebands, and strains

PSII electron flux (JV_{PSII}) measures the generation of reductant available to support biosynthetic assimilation and growth. JV_{PSII} was estimated using FRRf inductions with excitation at $\text{Ex}_{445\text{nm}}$, $\text{Ex}_{470\text{nm}}$, $\text{Ex}_{535\text{nm}}$, or $\text{Ex}_{590\text{nm}}$, corresponding to growth wavebands of 450, 470, 530, or 620 nm and 250 μM or 2.5 μM $[\text{O}_2]$. To focus on responses of growing cells, we do not present JV_{PSII} data for those PE-rich cultures which showed negligible growth under 405, 450, 730 nm and 250 μM O_2 ; nor for those PC-rich cultures which showed negligible growth under 405 nm and 250 μM O_2 . PSII electron flux (JV_{PSII} ; $\mu\text{mol e}^- \mu\text{mol Chl } a^{-1} \text{ s}^{-1}$) vs. Actinic PAR ($\mu\text{mol photons m}^{-2}\text{s}^{-1}$) estimated using FRRf induction curves with excitation at $\text{Ex}_{445\text{nm}}$, blue; $\text{Ex}_{470\text{nm}}$, blue-green; $\text{Ex}_{535\text{nm}}$, green; or $\text{Ex}_{590\text{nm}}$, orange; for PC-rich or PE-rich cultures of *Synechococcus* grown at spectral bandwidths of 450, 470, 530, or 620 nm and O_2 concentrations of 250 μM or 2.5 μM are also presented (Fig. S8).

Light response curves of PSII electron flux (JV_{PSII} ; $\mu\text{mol e}^- \mu\text{mol Chl } a^{-1} \text{ s}^{-1}$) vs. Actinic PAR ($\mu\text{mol photons m}^{-2}\text{s}^{-1}$) are shown in Fig. 4a. For the PC-rich strain, under all tested excitations ($\text{Ex}_{445\text{nm}}$, $\text{Ex}_{470\text{nm}}$, $\text{Ex}_{535\text{nm}}$, or $\text{Ex}_{590\text{nm}}$), JV_{PSII} increased with increasing Actinic PAR, and did not fully saturate across the range of tested actinic PAR. Under all excitations, except $\text{Ex}_{590\text{nm}}$, JV_{PSII} was higher at 2.5 μM $[\text{O}_2]$ compared to 250 μM $[\text{O}_2]$ for the PC-rich strain. Conversely, for the PE-rich strain, JV_{PSII} under $\text{Ex}_{470\text{nm}}$, $\text{Ex}_{535\text{nm}}$, or $\text{Ex}_{590\text{nm}}$ was higher at 250 μM $[\text{O}_2]$ compared to 2.5 μM $[\text{O}_2]$. Moreover, for the PE-rich strain, JV_{PSII} plateaued above $\sim 90 \mu\text{mol photons m}^{-2}\text{s}^{-1}$ under $\text{Ex}_{535\text{nm}}$, or $\text{Ex}_{590\text{nm}}$ for both low and high $[\text{O}_2]$. Strain, Actinic PAR, and $[\text{O}_2]$ significantly influence JV_{PSII} under some of the tested excitations (Table S9), but JV_{PSII} for cultures grown under, and excited through, $\text{Ex}_{445\text{nm}}$, absorbed by chlorophyll, shows no difference between low and high $[\text{O}_2]$ with increasing actinic light.

Fig. 4b presents linear regressions between chlorophyll-specific growth rates (μ ; d^{-1}) and cumulative diel PSII electron flux (JV_{PSII} ; $\mu\text{mol e}^- \mu\text{mol Chl } a^{-1} \text{ d}^{-1}$) measured under half ($90 \mu\text{mol photons m}^{-2}\text{s}^{-1}$) of the diel peak PAR growth light. μ (d^{-1}), as expected, was positively correlated with JV_{PSII} , with slopes significantly greater than 0. $[\text{O}_2]$ significantly influences the linear regressions between chlorophyll-specific growth rates and PSII electron flux for both PC-rich and PE-rich strains of *Synechococcus* ($p < 0.05$, Table S12). In the PC-rich strain higher $[\text{O}_2]$ increases the growth yield of electron transport. In contrast, the PE-rich strain, under higher $[\text{O}_2]$, decreases the growth yield of electron transport. However, the regressions for a given $[\text{O}_2]$ are not significantly different between the two strains ($p > 0.05$, Table S12).

Strain, actinic PAR waveband, and $[\text{O}_2]$ significantly influence Strain, Actinic PAR, and $[\text{O}_2]$ significantly influence our metric of Chl a : PSII (Fig. S9, Table S10), with Chl a : PSII higher

388 under 250 than under 2.5 μM $[\text{O}_2]$ in the PC-rich strain, and Chl *a* : PSII generally lower in the
389 PC-rich stain compared to the PE-rich strain.

390

Draft

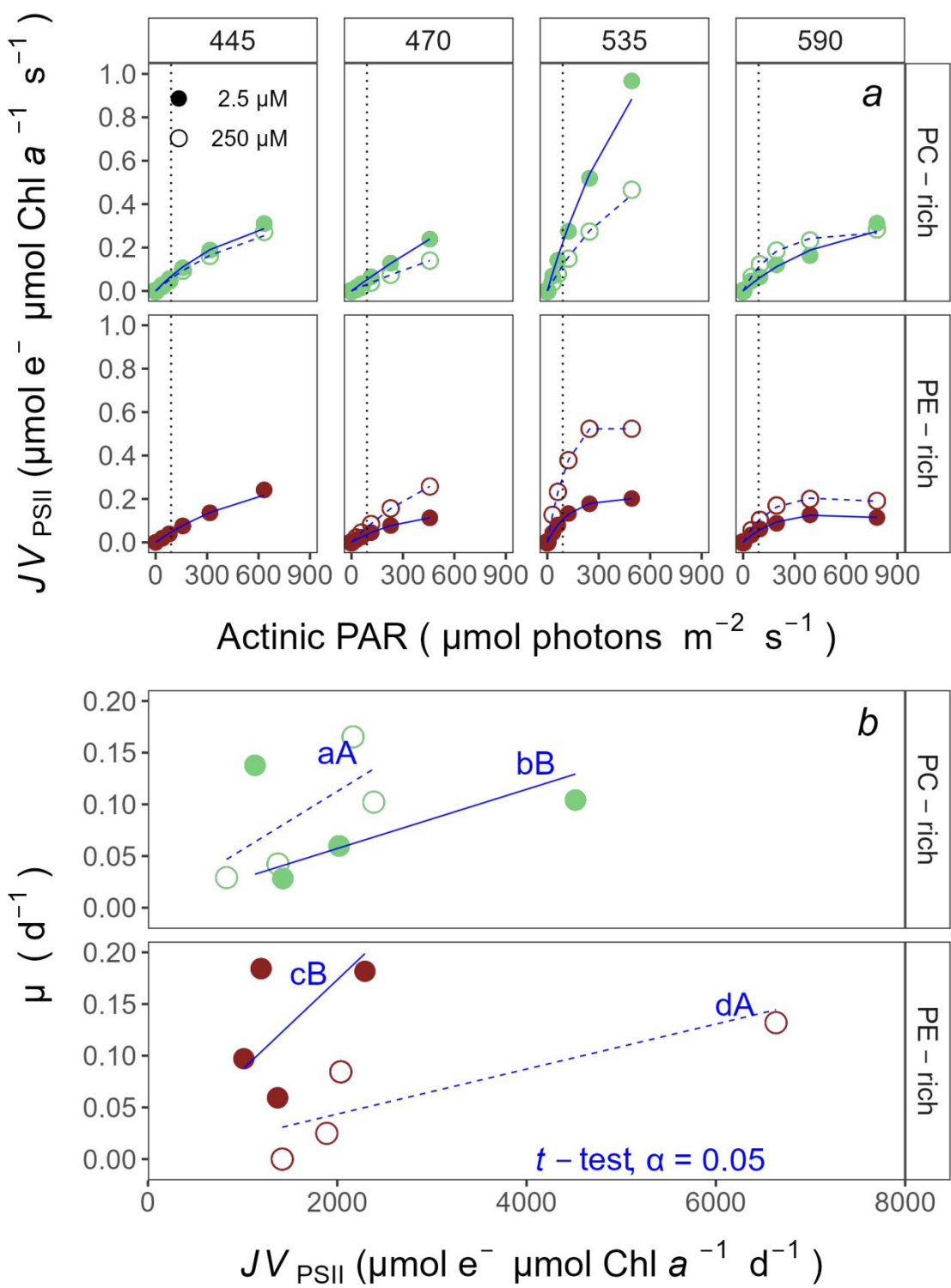


Fig. 4: PSII electron flux (JV_{PSII} ; $\mu\text{mol e}^- \mu\text{mol Chl } a^{-1} \text{ s}^{-1}$) vs. Actinic PAR ($\mu\text{mol photons m}^{-2} \text{ s}^{-1}$)

(a). JV_{PSII} was estimated using FRRf induction curves with excitation at $\text{Ex}_{445\text{nm}}$, blue; $\text{Ex}_{470\text{nm}}$,

blue-green; Ex_{535nm}, green; or Ex_{590nm}, orange; for PC-rich (green circle) or PE-rich (red circle) cultures of *Synechococcus*. Data show situations in which cultures were excited by, and growing in, corresponding growth wavebands of 450, 470, 530, or 620 nm and 250 μM [O₂] (open symbols and dashed line) or 2.5 μM [O₂] (closed symbols and solid line). JV_{PSII} vs. Actinic PAR ($\mu\text{mol photons m}^{-2}\text{s}^{-1}$) was fit with a Harrison and Platt Light Response Curve model (Harrison and Platt 1986), used to estimated JV_{PSII} at 90 $\mu\text{mol photons m}^{-2}\text{s}^{-1}$ (vertical dotted lines). Chlorophyll-specific growth rates ($\mu; \text{d}^{-1}$) vs. PSII electron flux ($JV_{\text{PSII}}; \mu\text{mol e}^{-} \mu\text{mol Chl } a^{-1} \text{d}^{-1}$) measured under half (90 $\mu\text{mol photons m}^{-2}\text{s}^{-1}$) of diel peak PAR growth light (*b*). Blue lines (solid for 2.5 μM [O₂] or dashed for 250 μM O₂) show linear model fit for data from each strain across spectral wavebands. Different blue lowercase letters indicate statistically significant differences between the fit models for different [O₂] within a given strain. Different blue uppercase letters indicate statistically significant differences between the fit models for different strains within a given [O₂] (*t*-test; $p < 0.05$).

Discussion

Growth responses of PC-rich and PE-rich picocyanobacteria across [O₂] and spectral wavebands

Picocyanobacteria from the genus *Synechococcus* are major contributors to primary marine production, across a wide range of environments (Śliwińska-Wilczewska et al. 2018a; Aguilera et al. 2023) but interactive influences of [O₂] and spectral wavebands on their growth rates and ecophysiology have not yet been investigated.

PC-rich and PE-rich *Synechococcus* from coastal habitats are exposed to changes in irradiance, spectral waveband, and sometimes [O₂], by vertical movements through the mixed

layer. Fluctuation in spectral wavebands changes the balance between productive photosynthesis, and photoinactivation of PSII (Six et al. 2007), increasing the cost of growth by diverting protein metabolism towards PSII repair (Murphy et al. 2017). Indeed, under 250 μM $[\text{O}_2]$, the PC-rich strain failed to grow under 405 nm, while the PE-rich strain failed to grow under 405 and 450, consistent with accelerated photoinactivation of PSII under blue wavebands (Murphy et al. 2017). In contrast, growth persisted in both strains at 405 & 450 nm under 2.5 μM $[\text{O}_2]$, likely because generation of toxic Reactive Oxygen Species (ROS) was suppressed, lowering the burden of photoinactivation of PSII.

μ shows positive responses to both Phycobiliproteins:Chlorophyll *a* ratio, an index of light capture capacity, and to cumulative diel PSII electron flux (JV_{PSII}) for *Synechococcus*, although the relations varied across strain and with $[\text{O}_2]$. In the PC-rich strain lower $[\text{O}_2]$ lowered the yield of growth per electron flux, while in the PE-rich strain the yield of growth per electron flux increased under lower $[\text{O}_2]$. Note that these regressions excluded those conditions where no growth occurred. In contrast, growth showed no correlation to estimated Photosynthetically Usable Radiation (PUR) (Fig. S4), likely because of variable allocations of excitation from phycobilisomes across growth conditions (Campbell 1996), not captured in the PUR metric based upon light absorption.

Wong et al. (2023) found that vertical structures of phytoplankton communities in OMZ are not sufficiently explained by top-down predation pressure nor light and/or nutrient limitation and thus, some phytoplankton may have a higher than expected direct O_2 requirement, with growth inhibited by low O_2 levels. However, in our work we show that low oxygen levels either do not suppress, and sometimes even benefit, growth of strains representing different *Synechococcus* pigment phenotypes across spectral wavebands. What is more, historical data link major extinction

events to warm climates and oxygen-deficient oceans, with current anthropogenic activities possibly leading to widespread OMZ within a thousand years (Breitburg et al. 2018). The PC-rich *Synechococcus* strain showed generally similar growth rates under high and low tested $[O_2]$, while the PE-rich strain achieved faster growth rates under low (2.5 μM) than under high (250 μM) $[O_2]$. PE-rich *Synechococcus* are typically found at greater depths, and lower light, than are PC-rich strains (Haverkamp et al. 2009; Śliwińska-Wilczewska et al. 2018a) but we suggest that at least some PE-rich strains may actually be limited to lower light niches by the interactions between light level, spectral band, and full air-saturated $[O_2]$. In lower oxygen waters some PE-rich strains may exploit higher light niches nearer the surface.

Physiological adaptations of PC-rich and PE-rich picocyanobacteria to $[O_2]$ and spectral wavebands

Synechococcus strains vary widely in pigment composition, enabling them to exploit different spectral niches (Moore et al. 1995; Six et al. 2007; Grébert et al. 2018; Efimova et al. 2020). With a small diameter of 0.8–2.0 μm , *Synechococcus* possess a high surface-to-volume ratio (Śliwińska-Wilczewska et al. 2018b), minimizing pigment package effects (Finkel 2001), and resulting in high optical absorption per pigment. This characteristic allows them to thrive under low light deep in the water column (Moore et al. 1995), and to disproportionately influence subsurface light fields (Berthold and Schumann 2020). Although limited package effect increases photon capture per pigment investment, it also increases *Synechococcus* susceptibility to light-induced damage (Llabrés and Agustí 2006, 2010). In some *Synechococcus*, a carotenoid-protein complex regulates the connectivity of the phycobilisome to the reaction center, mediating a form of non-photochemical quenching of excitation (Wilson et al. 2006; Gorbunov et al. 2011;

Kirilovsky 2015). In our work we found no change in bulk carotenoids content (Fig. 2), nor in Car to Chl *a* ratio (Fig. S3) under the different [O₂]. What is more, for the chosen PE-rich strain, the carotenoids content did not change across tested wavebands. On the other hand, for the chosen PC-rich strain, a slight increase in carotenoids content was recorded under 405 nm, although these cells were not growing and were thus under stress.

σ_{PSII} was low and showed little change with increasing actinic light during excitation through chlorophyll at Ex_{445nm}, because in cyanobacteria the number of chlorophyll per PSII is low, and nearly fixed, so the effective absorption cross section of PSII for chlorophyll is low (Xu et al. 2018). With excitation through the phycobilisomes at 535 and 590 nm σ_{PSII} rose to a peak near the acclimated light level of $\sim 90 \mu\text{mol photons m}^{-2}\text{s}^{-1}$ (Campbell and Oquist 1996), reflecting the state transition from State II in the dark towards State I near the growth light level, with subsequent decrease in σ_{PSII} , as excitation is again directed away from PSII.

τ_{PSII} was generally faster for both the chosen PC-rich and PE-rich strains under 250 μM [O₂], consistent with the cyanobacterial capacity for pseudo-cyclic electron flows away from PSII to [O₂] (Campbell et al. 1999; Grossman et al. 2010; Allahverdiyeva et al. 2015; Hughes et al. 2018), thereby controlling feedback inhibition of electron transport. In parallel, q_{P} was generally higher for the PC-rich, and particularly for the PE-rich strain, under 250 μM [O₂], since cyanobacteria show strong capacity for electron flow away from PSII to O₂ (Campbell et al. 1999; Hughes et al. 2018), particularly under excess excitation above the acclimated PAR of $\sim 90 \mu\text{mol photons m}^{-2}\text{s}^{-1}$. In spite of this faster electron transport performance under 250 μM [O₂] the PE-rich strain grew faster under 2.5 μM [O₂], showing an increase in the growth return upon electron transport, possibly because of a decrease in metabolic burden, through suppression of ROS formation under

lower [O₂]. Future genomic comparisons may uncover the bases for these distinct strain responses to changing [O₂].

Picocyanobacteria numerically dominate vast tracts of the oceans, contributing significant primary production, particularly in oligotrophic regions, but also some coastal habitats (Haverkamp 2008; Larsson et al. 2014; Doré et al. 2022; Aguilera et al. 2023). The ecological success of picoplanktonic *Synechococcus* reflects specific lineages occupying different niches to populate the world's oceans (Scanlan 2012). Picocyanobacteria species can share the light spectrum by specializing in different wavelengths (Stomp et al. 2004, 2007; Haverkamp et al. 2009). Competition models and laboratory experiments show that PE-rich picocyanobacteria outperform competitors in green light while PC-rich picocyanobacteria dominate in red light, while both species can coexist across the full spectrum (Stomp et al. 2004, 2007). We now find that spectral wavebands interact with [O₂] as determinants of growth rates across PE- and PC-rich strains of *Synechococcus*, and that changing ocean [O₂] might drive strains of different pigmentation phenotypes into changing ecological niches.

Acknowledgements

We would like to express our sincere gratitude to the Editor, and two Reviewers for their efforts reviewing and improving this manuscript. We thank Naaman M. Omar for assistance with coding, data analyses and culture maintenance; Miranda Corkum who maintained cultures and trained personnel in culture handling; Laurel Genge, and Carlie Barnhill (Mount Allison students) who assisted with R code.

Article information

Data availability statement

Data supporting this study is available on: <https://github.com/FundyPhytoPhys/BalticO2> (public GitHub Repository) and https://docs.google.com/spreadsheets/d/1ZXpwR7Gfto-uRzVdXzMpQF4frbrvMLH_IyLqonFZRSw/edit#gid=0 (URL for MetaDataCatalog).

Code to perform data processing and analyses is available at <https://github.com/FundyPhytoPhys/BalticO2>.

Author information

Author ORCIDs

Sylwia Śliwińska-Wilczewska <https://orcid.org/0000-0002-3147-6605> Mireille Savoie <https://orcid.org/0009-0009-9499-6657> Douglas A. Campbell <https://orcid.org/0000-0001-8996-5463>

Author contributions

Conceptualization: SSW, DAC Data curation: SSW Formal analysis: SSW, MS, DAC Funding acquisition: DAC Investigation: SSW Methodology: SSW, MS, DAC Project administration: DAC Resources: DAC Supervision: DAC Validation: SSW, MS, DAC Visualization: SSW Writing – original draft: SSW, MS, DAC

Competing interests

The authors declare there are no competing interests.

Funding information

This work was supported by Canada Research Chair in Phytoplankton Ecophysiology (DAC) and Latitude & Light; NSERC of Canada Discovery Grant (DAC).

Supplementary material

Supplementary data are available with the article at <https://github.com/FundyPhytoPhys/BalticO2>.

References

- Aguilera, A., Alegria Zufia, J., Bas Conn, L., Gurlit, L., Śliwińska-Wilczewska, S., Budzałek, G., Lundin, D., Pinhassi, J., Legrand, C., and Farnelid, H. 2023. Ecophysiological analysis reveals distinct environmental preferences in closely related Baltic Sea picocyanobacteria. *Environmental Microbiology* **25**(9): 1674–1695. doi:10.1111/1462-2920.16384.
- Allahverdiyeva, Y., Isojärvi, J., Zhang, P., and Aro, E.-M. 2015. Cyanobacterial Oxygenic Photosynthesis is Protected by Flavodiiron Proteins. *Life* **5**(1): 716–743. Multidisciplinary Digital Publishing Institute. doi:10.3390/life5010716.
- Andersson, B., Salter, A.H., Virgin, I., Vass, I., and Styring, S. 1992. Photodamage to photosystem II - primary and secondary events. *Journal of Photochemistry and Photobiology B: Biology* **15**(1): 15–31. doi:10.1016/1011-1344(92)87003-R.
- Bagby, S.C., and Chisholm, S.W. 2015. Response of *Prochlorococcus* to varying CO₂:O₂ ratios. *The ISME Journal* **9**(10): 2232–2245. doi:10.1038/ismej.2015.36.

- 551 Bennett, A., and Bogorad, L. 1973. Complementary Chromatic Adaptation in a filamentous blue-
552 green alga. *Journal of Cell Biology* **58**(2): 419–435. doi:10.1083/jcb.58.2.419.
- 553 Berthold, M., and Schumann, R. 2020. Phosphorus Dynamics in a Eutrophic Lagoon: Uptake and
554 Utilization of Nutrient Pulses by Phytoplankton. *Frontiers in Marine Science* **7**. Frontiers.
555 doi:10.3389/fmars.2020.00281.
- 556 Blake, R., and Griff, M. 2012. In situ spectroscopy on intact *Leptospirillum Ferrooxidans* reveals
557 that reduced cytochrome 579 is an obligatory intermediate in the aerobic iron respiratory chain.
558 *Frontiers in Microbiology* **3**. [accessed 13 June 2023].
- 559 Boatman, T.G., Geider, R.J., and Oxborough, K. 2019. Improving the accuracy of Single Turnover
560 Active Fluorometry (STAF) for the estimation of Phytoplankton Primary Productivity (PhytoPP).
561 *Frontiers in Marine Science* **6**. Frontiers. doi:10.3389/fmars.2019.00319.
- 562 Breitburg, D., Levin, L.A., Oschlies, A., Grégoire, M., Chavez, F.P., Conley, D.J., Garçon, V.,
563 Gilbert, D., Gutiérrez, D., Isensee, K., Jacinto, G.S., Limburg, K.E., Montes, I., Naqvi, S.W.A.,
564 Pitcher, G.C., Rabalais, N.N., Roman, M.R., Rose, K.A., Seibel, B.A., Telszewski, M., Yasuhara,
565 M., and Zhang, J. 2018. Declining oxygen in the global ocean and coastal waters. *Science*
566 **359**(6371): eaam7240. American Association for the Advancement of Science.
567 doi:10.1126/science.aam7240.
- 568 Callieri, C., Cabello-Yeves, P.J., and Bertoni, F. 2022. The “Dark Side” of Picocyanobacteria: Life
569 as We Do Not Know It (Yet). *Microorganisms* **10**(3): 546. Multidisciplinary Digital Publishing
570 Institute. doi:10.3390/microorganisms10030546.

- 571 Campbell, D. 1996. Complementary chromatic adaptation alters photosynthetic strategies in the
572 cyanobacterium *Calothrix*. *Microbiology* **142**(5): 1255–1263. Microbiology Society,.
573 doi:10.1099/13500872-142-5-1255.
- 574 Campbell, D., Clarke, A.K., Gustafsson, P., and Öquist, G. 1999. Oxygen-dependent electron flow
575 influences photosystem II function and *psbA* gene expression in the cyanobacterium
576 *Synechococcus* sp. PCC 7942. *Physiologia Plantarum* **105**(4): 746–755. doi:10.1034/j.1399-
577 3054.1999.105420.x.
- 578 Campbell, D., and Oquist, G. 1996. Predicting Light Acclimation in Cyanobacteria from
579 Nonphotochemical Quenching of Photosystem II Fluorescence, Which Reflects State Transitions
580 in These Organisms. *Plant Physiology* **111**(4): 1293–1298. doi:10.1104/pp.111.4.1293.
- 581 Doré, H., Leconte, J., Guyet, U., Breton, S., Farrant, G.K., Demory, D., Ratin, M., Hoebeke, M.,
582 Corre, E., Pitt, F.D., Ostrowski, M., Scanlan, D.J., Partensky, F., Six, C., and Garczarek, L. 2022.
583 Global Phylogeography of Marine *Synechococcus* in Coastal Areas Reveals Strong Community
584 Shifts. *mSystems* **7**(6): e00656–22. American Society for Microbiology.
585 doi:10.1128/msystems.00656-22.
- 586 Efimova, T.V., Churilova, T.Ya., and Mukhanov, V.S. 2020. The Influence of Light of Different
587 Spectral Qualities on the Photosynthetic Characteristics of C-Phycocyanine-Containing
588 Cyanobacteria *Synechococcus* sp. WH5701. *Russian Journal of Marine Biology* **46**(2): 105–112.
589 doi:10.1134/S1063074020020042.
- 590 Elzhov, T.V., Mullen, K.M., Spiess, A.-N., and Bolker, B. 2023, September. Minpack.lm: R
591 Interface to the Levenberg-Marquardt Nonlinear Least-Squares Algorithm Found in MINPACK,
592 Plus Support for Bounds. [accessed 15 March 2024].

- 593 Falkowski, P.G., Katz, M.E., Knoll, A.H., Quigg, A., Raven, J.A., Schofield, O., and Taylor, F.J.R.
594 2004. The Evolution of Modern Eukaryotic Phytoplankton. *Science* **305**(5682): 354–360.
595 American Association for the Advancement of Science. doi:10.1126/science.1095964.
- 596 Falkowski, P., and Kolber, Z. 1993. Estimation of phytoplankton photosynthesis by active
597 fluorescence. *ICES Marine Science Symposium* **197**: 92–103.
- 598 Finkel, Z.V. 2001. Light absorption and size scaling of light-limited metabolism in marine
599 diatoms. *Limnology and Oceanography* **46**(1): 86–94. doi:10.4319/lo.2001.46.1.0086.
- 600 Flombaum, P., Gallegos, J.L., Gordillo, R.A., Rincón, J., Zabala, L.L., Jiao, N., Karl, D.M., Li,
601 W.K.W., Lomas, M.W., Veneziano, D., Vera, C.S., Vrugt, J.A., and Martiny, A.C. 2013. Present
602 and future global distributions of the marine Cyanobacteria *Prochlorococcus* and *Synechococcus*.
603 *Proceedings of the National Academy of Sciences* **110**(24): 9824–9829. *Proceedings of the*
604 *National Academy of Sciences*. doi:10.1073/pnas.1307701110.
- 605 Gorbunov, M.Y., Kuzminov, F.I., Fadeev, V.V., Kim, J.D., and Falkowski, P.G. 2011. A kinetic
606 model of non-photochemical quenching in cyanobacteria. *Biochimica et Biophysica Acta (BBA)*
607 *- Bioenergetics* **1807**(12): 1591–1599. doi:10.1016/j.bbabi.2011.08.009.
- 608 Grébert, T., Doré, H., Partensky, F., Farrant, G.K., Boss, E.S., Picheral, M., Guidi, L., Pesant, S.,
609 Scanlan, D.J., Wincker, P., Acinas, S.G., Kehoe, D.M., and Garczarek, L. 2018. Light color
610 acclimation is a key process in the global ocean distribution of *Synechococcus* cyanobacteria.
611 *Proceedings of the National Academy of Sciences* **115**(9): E2010–E2019. *Proceedings of the*
612 *National Academy of Sciences*. doi:10.1073/pnas.1717069115.

- Grossman, A.R., Mackey, K.R.M., and Bailey, S. 2010. A Perspective on Photosynthesis in the Oligotrophic Oceans: Hypotheses Concerning Alternate Routes of Electron Flow¹. *Journal of Phycology* **46**(4): 629–634. doi:10.1111/j.1529-8817.2010.00852.x.
- Guillard, R.R.L. 1975. Culture of phytoplankton for feeding marine invertebrates. *In* *Culture of Marine Invertebrate Animals: Proceedings — 1st Conference on Culture of Marine Invertebrate Animals Greenport. Edited by* W.L. Smith and M.H. Chanley. Springer US, Boston, MA. pp. 29–60. doi:10.1007/978-1-4615-8714-9_3.
- Hakala, M., Tuominen, I., Keränen, M., Tyystjärvi, T., and Tyystjärvi, E. 2005. Evidence for the role of the oxygen-evolving manganese complex in photoinhibition of Photosystem II. *Biochimica et Biophysica Acta (BBA) - Bioenergetics* **1706**(1): 68–80. doi:10.1016/j.bbabi.2004.09.001.
- Handel, A. 2020, October. Andreas Handel - Custom Word formatting using R Markdown. <https://www.andreashandel.com/posts/2020-10-07-custom-word-format/>. [accessed 13 June 2023].
- Harrison, W.G., and Platt, T. 1986. Photosynthesis-irradiance relationships in polar and temperate phytoplankton populations. *Polar biology* **5**: 153–164. Springer. [accessed 15 March 2024].
- Haverkamp, T.H.A. 2008. Shades of red and green : The colorful diversity and ecology of picocyanobacteria in the Baltic Sea. Yerseke Netherlands Institute of Ecology (NIOO) - Royal Netherlands Academy of Arts and Sciences. [accessed 3 July 2024].
- Haverkamp, T.H.A., Schouten, D., Doeleman, M., Wollenzien, U., Huisman, J., and Stal, L.J. 2009. Colorful microdiversity of *Synechococcus* strains (picocyanobacteria) isolated from the Baltic Sea. *The ISME Journal* **3**(4): 397–408. doi:10.1038/ismej.2008.118.

- 634 Hughes, D.J., Campbell, D.A., Doblin, M.A., Kromkamp, J.C., Lawrenz, E., Moore, C.M.,
635 Oxborough, K., Prášil, O., Ralph, P.J., Alvarez, M.F., and Suggett, D.J. 2018. Roadmaps and
636 Detours: Active Chlorophyll-a Assessments of Primary Productivity Across Marine and
637 Freshwater Systems. *Environmental Science & Technology* **52**(21): 12039–12054. American
638 Chemical Society. doi:10.1021/acs.est.8b03488.
- 639 Jávorfí, T., Erostyák, J., Gál, J., Buzády, A., Menczel, L., Garab, G., and Razi Naqvi, K. 2006.
640 Quantitative spectrophotometry using integrating cavities. *Journal of Photochemistry and*
641 *Photobiology B: Biology* **82**(2): 127–131. doi:10.1016/j.jphotobiol.2005.10.002.
- 642 Keeling, R.F., Körtzinger, A., and Gruber, N. 2010. Ocean Deoxygenation in a Warming World.
643 *Annual Review of Marine Science* **2**(Volume 2, 2010): 199–229. Annual Reviews.
644 doi:10.1146/annurev.marine.010908.163855.
- 645 Kirilovsky, D. 2015. Modulating energy arriving at photochemical reaction centers: Orange
646 carotenoid protein-related photoprotection and state transitions. *Photosynthesis Research* **126**(1):
647 3–17. doi:10.1007/s11120-014-0031-7.
- 648 Kolber, Z.S., Prášil, O., and Falkowski, P.G. 1998. Measurements of variable chlorophyll
649 fluorescence using fast repetition rate techniques: Defining methodology and experimental
650 protocols. *Biochimica et Biophysica Acta (BBA) - Bioenergetics* **1367**(1): 88–106.
651 doi:10.1016/S0005-2728(98)00135-2.
- 652 Larsson, J., Celepli, N., Ininbergs, K., Dupont, C.L., Yooseph, S., Bergman, B., and Ekman, M.
653 2014. Picocyanobacteria containing a novel pigment gene cluster dominate the brackish water
654 Baltic Sea. *The ISME Journal* **8**(9): 1892–1903. doi:10.1038/ismej.2014.35.

- 655 Latala, A., Jodłowska, S., and Pniewski, F. 2006. Culture Collection of Baltic Algae (CCBA) and
656 characteristic of some strains by factorial experiment approach. *Archiv fur Hydrobiologie* **122**:
657 137–154. [accessed 19 June 2024].
- 658 Llabrés, M., and Agustí, S. 2006. Picophytoplankton cell death induced by UV radiation: Evidence
659 for oceanic Atlantic communities. *Limnology and Oceanography* **51**(1): 21–29.
660 doi:10.4319/lo.2006.51.1.0021.
- 661 Llabrés, M., and Agustí, S. 2010. Effects of ultraviolet radiation on growth, cell death and the
662 standing stock of Antarctic phytoplankton. *Aquatic Microbial Ecology* **59**(2): 151–160.
663 doi:10.3354/ame01392.
- 664 Luimstra, V.M., Schuurmans, J.M., Verschoor, A.M., Hellingwerf, K.J., Huisman, J., and
665 Matthijs, H.C.P. 2018. Blue light reduces photosynthetic efficiency of cyanobacteria through an
666 imbalance between photosystems I and II. *Photosynthesis Research* **138**(2): 177–189.
667 doi:10.1007/s11120-018-0561-5.
- 668 Moore, L.R., Goericke, R., and Chisholm, S.W. 1995. Comparative physiology of *Synechococcus*
669 and *Prochlorococcus*: Influence of light and temperature on growth, pigments, fluorescence and
670 absorptive properties. *Marine Ecology Progress Series* **116**(1/3): 259–275. Inter-Research Science
671 Center. Available from <https://www.jstor.org/stable/44635011> [accessed 1 July 2024].
- 672 Morel, A. 1978. Available, usable, and stored radiant energy in relation to marine photosynthesis.
673 *Deep Sea Research* **25**(8): 673–688. doi:10.1016/0146-6291(78)90623-9.

- 674 Murphy, C.D., Roodvoets, M.S., Austen, E.J., Dolan, A., Barnett, A., and Campbell, D.A. 2017.
675 Photoinactivation of Photosystem II in *Prochlorococcus* and *Synechococcus*. *PLOS ONE* **12**(1):
676 e0168991. Public Library of Science. doi:10.1371/journal.pone.0168991.
- 677 Oxborough, K., and Baker, N.R. 1997. Resolving chlorophyll *a* fluorescence images of
678 photosynthetic efficiency into photochemical and non-photochemical components – calculation of
679 qP and F_v/F_m ; without measuring F_o ; *Photosynthesis Research* **54**(2): 135–142.
680 doi:10.1023/A:1005936823310.
- 681 Oxborough, K., Moore, C.M., Suggett, D.J., Lawson, T., Chan, H.G., and Geider, R.J. 2012. Direct
682 estimation of functional PSII reaction center concentration and PSII electron flux on a volume
683 basis: A new approach to the analysis of Fast Repetition Rate fluorometry (FRRf) data. *Limnology*
684 *and Oceanography: Methods* **10**(3): 142–154. doi:10.4319/lom.2012.10.142.
- 685 Partensky, F., Mella-Flores, D., Six, C., Garczarek, L., Czjzek, M., Marie, D., Kotabová, E.,
686 Felcmanová, K., and Prášil, O. 2018. Comparison of photosynthetic performances of marine
687 picocyanobacteria with different configurations of the oxygen-evolving complex. *Photosynthesis*
688 *Research* **138**(1): 57–71. doi:10.1007/s11120-018-0539-3.
- 689 Pedersen, T.L. 2024, January. Patchwork: The Composer of Plots. [accessed 20 April 2024].
- 690 Posit team. 2022. RStudio: Integrated development environment for r. Posit Software, PBC,
691 Boston, MA. Available from <http://www.posit.co/>.
- 692 R Core Team. 2023. R: A language and environment for statistical computing. R Foundation for
693 Statistical Computing, Vienna, Austria. Available from <https://www.R-project.org/>.

- 694 Scanlan, D.J. 2012. Marine Picocyanobacteria. *In* Ecology of Cyanobacteria II: Their Diversity in
695 Space and Time. *Edited by* B.A. Whitton. Springer Netherlands, Dordrecht. pp. 503–533.
696 doi:10.1007/978-94-007-3855-3_20.
- 697 Six, C., Finkel, Z.V., Irwin, A.J., and Campbell, D.A. 2007. Light variability illuminates niche-
698 partitioning among marine picocyanobacteria. PLOS ONE **2**(12): e1341. Public Library of
699 Science. doi:10.1371/journal.pone.0001341.
- 700 Śliwińska-Wilczewska, S., Cieszyńska, A., Maculewicz, J., and Latała, A. 2018a.
701 Ecophysiological characteristics of red, green, and brown strains of the Baltic picocyanobacterium
702 *Synechococcus* sp. – a laboratory study. Biogeosciences **15**(20): 6257–6276. Copernicus GmbH.
703 doi:10.5194/bg-15-6257-2018.
- 704 Śliwińska-Wilczewska, S., Maculewicz, J., Barreiro Felpeto, A., and Latała, A. 2018b.
705 Allelopathic and bloom-forming picocyanobacteria in a changing world. Toxins **10**(1): 48.
706 Multidisciplinary Digital Publishing Institute. doi:10.3390/toxins10010048.
- 707 Stomp, M., Huisman, J., de Jongh, F., Veraart, A.J., Gerla, D., Rijkeboer, M., Ibelings, B.W.,
708 Wollenzien, U.I.A., and Stal, L.J. 2004. Adaptive divergence in pigment composition promotes
709 phytoplankton biodiversity. Nature **432**(7013): 104–107. Nature Publishing Group.
710 doi:10.1038/nature03044.
- 711 Stomp, M., Huisman, J., Vörös, L., Pick, F.R., Laamanen, M., Haverkamp, T., and Stal, L.J. 2007.
712 Colourful coexistence of red and green picocyanobacteria in lakes and seas. Ecology Letters **10**(4):
713 290–298. doi:10.1111/j.1461-0248.2007.01026.x.

- 714 Strickland, J.D., and Parsons, T.R. 1972. Practical Hand Book of Seawater Analysis. Fisheries
715 Research Board of Canada **167 (2nd edition)**: 1–311. doi:DOI: [http://dx.doi.org/10.25607/OBP-](http://dx.doi.org/10.25607/OBP-1791)
716 1791.
- 717 Tortell, P., and Suggett, D.J. 2021. A user guide for the application of Single Turnover active
718 chlorophyll fluorescence for phytoplankton productivity measurements. Version 1. Report,
719 Scientific Committee on Oceanic Research (SCOR) Working Group 156. doi:10.25607/OBP-
720 1084.
- 721 Ulloa, O., Canfield, D.E., DeLong, E.F., Letelier, R.M., and Stewart, F.J. 2012. Microbial
722 oceanography of anoxic oxygen minimum zones. *Proceedings of the National Academy of*
723 *Sciences* **109**(40): 15996–16003. *Proceedings of the National Academy of Sciences*.
724 doi:10.1073/pnas.1205009109.
- 725 Ulloa, O., Henríquez-Castillo, C., Ramírez-Flandes, S., Plominsky, A.M., Murillo, A.A., Morgan-
726 Lang, C., Hallam, S.J., and Stepanauskas, R. 2021. The cyanobacterium *Prochlorococcus* has
727 divergent light-harvesting antennae and may have evolved in a low-oxygen ocean. *Proceedings of*
728 *the National Academy of Sciences* **118**(11): e2025638118. *Proceedings of the National Academy*
729 *of Sciences*. doi:10.1073/pnas.2025638118.
- 730 Wickham, H. 2016. Data Analysis. *In* *Ggplot2: Elegant Graphics for Data Analysis*. *Edited by* H.
731 Wickham. Springer International Publishing, Cham. pp. 189–201. doi:10.1007/978-3-319-24277-
732 4_9.
- 733 Wilson, A., Ajlani, G., Verbavatz, J.-M., Vass, I., Kerfeld, C.A., and Kirilovsky, D. 2006. A
734 Soluble Carotenoid Protein Involved in Phycobilisome-Related Energy Dissipation in
735 Cyanobacteria. *The Plant Cell* **18**(4): 992–1007. doi:10.1105/tpc.105.040121.

- 736 Włodkowiec, D., Czerw, A., Karakiewicz, B., and Deptała, A. 2022. Recent progress in cytometric
737 technologies and their applications in ecotoxicology and environmental risk assessment.
738 *Cytometry Part A* **101**(3): 203–219. doi:10.1002/cyto.a.24508.
- 739 Wong, J.C.Y., Raven, J.A., Aldunate, M., Silva, S., Gaitán-Espitia, J.D., Vargas, C.A., Ulloa, O.,
740 and von Dassow, P. 2023. Do phytoplankton require oxygen to survive? A hypothesis and model
741 synthesis from oxygen minimum zones. *Limnology and Oceanography* **68**(7): 1417–1437.
742 doi:10.1002/lno.12367.
- 743 Xu, K., Grant-Burt, J.L., Donaher, N., and Campbell, D.A. 2017. Connectivity among
744 Photosystem II centers in phytoplankters: Patterns and responses. *Biochimica et Biophysica Acta*
745 (BBA) - Bioenergetics **1858**(6): 459–474. doi:10.1016/j.bbabo.2017.03.003.
- 746 Xu, K., Lavaud, J., Perkins, R., Austen, E., Bonnanfant, M., and Campbell, D.A. 2018.
747 Phytoplankton σ_{PSII} and excitation dissipation; implications for estimates of primary
748 productivity. *Frontiers in Marine Science* **5**. doi:10.3389/fmars.2018.00281.

Coastal *Synechococcus* strains can exploit low oxygen habitats

Sylvia Śliwińska-Wilczewska^{1,2}, Mireille Savoie¹, and Douglas A. Campbell^{1,✉}

¹ Department of Biology, Mount Allison University, 53 York St., Sackville, NB, E4L 1C9, Canada

² Institute of Oceanography, University of Gdansk, 46 Pilsudskiego St, P81-378, Gdynia, Poland

✉ Correspondence: Douglas A. Campbell <dubhglascambeuil@gmail.com>

Abstract

We found that PhycoErythrin-rich *Synechococcus* achieved faster growth rates (μ), across the spectral bandwidths from 405 – 730 nm, under 2.5 μM $[\text{O}_2]$, characteristic of Oxygen Minimum Zones (OMZs), than under 250 μM $[\text{O}_2]$, whereas PhycoCyanin-rich strain showed generally similar μ under 2.5 and 250 μM $[\text{O}_2]$. For PhycoCyanin- and PhycoErythrin-rich *Synechococcus*, μ showed also positive linear responses to both Phycobiliproteins:Chlorophyll *a*, and to cumulative diel PSII electron flux, although the relations vary across strain and $[\text{O}_2]$. Electron transport downstream of Photosystem II was generally higher for both PhycoCyanin- and PhycoErythrin-rich strains under 250 μM $[\text{O}_2]$, since cyanobacteria show strong capacity for electron flow away from PSII to O_2 , particularly under excess excitation. Even though electron transport was faster under 250 μM $[\text{O}_2]$, the PhycoErythrin-rich strain showed a higher growth yield of electron transport under 2.5 μM $[\text{O}_2]$. PhycoErythrin-rich *Synechococcus* are currently typically found at greater depths, and lower light, than are PhycoCyanin-rich strains, but we suggest that the PhycoErythrin-rich strains are actually limited to lower light by an interaction

between light and full air-saturated [O₂]. In expanding Oxygen Minimum Zones PhycoErythrin-rich strains will likely exploit higher light niches, across a wider spectral range.

Key words: Colour, niches, OMZs, oxygen concentration, PC-rich strain, PE-rich strain, spectral wavebands, *Synechococcus*

Introduction

Since the mid-20th century, declining oxygen concentrations in regions of the open ocean, and in coastal waters (Breitburg et al. 2018) are affecting productivity, biodiversity, and biogeochemical cycles in marine ecosystems (Keeling et al. 2010). Low oxygen environments in the ocean, termed Oxygen Minimum Zones (OMZ) have expanded to an area equivalent to the European Union, and the global volume of oxygen-free water has quadrupled (Breitburg et al. 2018). It is thus necessary to understand which species will survive and dominate under ongoing and predicted changes in ocean and coastal oxygen concentrations.

Oxygenic picocyanobacteria numerically dominate the phytoplankton across vast tracts of the world's oceans, notably in oligotrophic regions, but also in some coastal ecosystems (Larsson et al. 2014; Śliwińska-Wilczewska et al. 2018a; Aguilera et al. 2023). Oxygen is a product of photosynthesis, and a substrate for reductant consumption, but also has potential to damage Photosystem II (PSII) protein subunits (Andersson et al. 1992). The oxygen evolving complex of PSII can also be directly inactivated by a photon in the UV or blue range directly absorbed by the Mn₄Ca cluster (Hakala et al. 2005; Partensky et al. 2018); therefore, oxygen interacts with spectral band to influence the balance between productive photosynthesis and costly photoinactivations (Murphy et al. 2017). OMZ pose challenges for aerobic organisms (Breitburg et al. 2018), but

picocyanobacteria inhabiting OMZs have genetic adaptations enabling them to tolerate and even thrive in oxygen-depleted environments, such as changes in energy metabolism, antioxidant defense mechanisms, and cellular structures optimized for oxygen scavenging and storage (Ulloa et al. 2012, 2021; Bagby and Chisholm 2015; Partensky et al. 2018; Callieri et al. 2022; Wong et al. 2023).

Picocyanobacteria also show photosynthetic adaptations to spectral wavebands, ranging from short-wavelength blue light (Luimstra et al. 2018), through green and yellow light to long-wavelength red light. Plankton ecologists have long acknowledged that a diverse array of photosynthetic pigments allows cyanobacteria species to exploit different spectral wavebands (Falkowski et al. 2004; Stomp et al. 2007). The ecological success of picoplanktonic *Synechococcus* strains throughout the photic oceanic water column (Flombaum et al. 2013) results in part from diverse strategies to respond to variations in their environment (Scanlan 2012; Doré et al. 2020). The genus *Synechococcus* is genetically diverse and divided into several major clusters. Picocyanobacteria from *Synechococcus* cluster 5, often found in marine, brackish and freshwater environments (Sánchez-Baracaldo et al. 2019; Aguilera et al. 2023), includes sub-clusters of strains rich in phycoerythrin (PE-rich), which imparts a range of orange, reddish, pink, and purple colors, as well as sub-clusters of strains rich in phycocyanin (PC-rich), which color the organism in various shades of blue-green (Stomp et al. 2004). Competition experiments demonstrate that PC-rich and PE-rich strains can coexist in white light but show spectral niche differentiation (Haverkamp 2008; Callieri et al. 2012).

PE-rich strains, with high content of the chromophore phycourobilin (PUB), dominate oligotrophic deep waters where blue light predominates, and deep communities in more mesotrophic marine waters, characterized by blue-green light environments (Stomp et al. 2004;

Haverkamp et al. 2009) are shifting towards PE-rich *Synechococcus* with more phycoerythrobilin (PEB). Conversely, PC-rich strains prevail near the surface, and in turbid waters where orange and red light dominate. The widespread coexistence of PC-rich and PE-rich picocyanobacteria is observed in waters of intermediate turbidity, such as mesotrophic lakes and coastal seas (Haverkamp 2008; Haverkamp et al. 2009).

Our aim was to test the growth and functional responses of PC-rich and PE-rich *Synechococcus* cultures to the interaction of different oxygen concentrations (250 μM or 2.5 μM $[\text{O}_2]$), and spectral wavebands (405 – 730 nm). We thus empirically answer the question posed by Wong et al. (2023) regarding the sensitivity of modern picocyanobacteria to low levels of O_2 and a wide range of wavebands found across depths and trophic levels.

Materials and methods

Culture condition and experimental setup

Xenic cultures of PC-rich (CCBA_077) and PE-rich (CCBA_127) *Synechococcus* were obtained from the Culture Collection of Baltic Algae (<https://ccba.ug.edu.pl/pages/en/home.php>) (Latala et al. 2006). *Synechococcus* strains were cultured in Tissue Culture Flasks (VWR International, Cat. No. 10062-872, PA, USA) and transferred biweekly to fresh f/2 media (Guillard 1975) prepared at a salinity of 8 PSU, reflective of their natural brackish habitat. Pre-cultures were maintained in incubators with full air saturated dissolved oxygen concentration $[\text{O}_2]$ of 250 μM , 22°C, with a light/dark cycle of 12 hours (h) and Photosynthetically Active Radiation (PAR) of 10 $\mu\text{mol photons m}^{-2}\text{s}^{-1}$ from Philips Cool White F14T5/841 Alto, 14 watts, fluorescent bulbs.

Controlled growth experiments were performed using MCMIX-OD PSI Multicultivators (Photon Systems Instruments, Drásov, Czech Republic) set to 22°C. Each of 8 round bottom

cylindrical glass tubes contained 75 mL of f/2 medium and 5 mL of growing pre-culture. These parameters allowed for exponential growth of the cultures from the beginning of the experiment, with little lag phase. Inoculation of culture tubes took place in the afternoon, with a period of low light and then 12 h darkness before a sinusoidal 12 h photoperiod cycle commenced at 07:00 the following morning, with peak PAR of $180 \mu\text{mol photons m}^{-2}\text{s}^{-1}$ reached at 13:00 each day.

Each tube was maintained under an individual combination of one of 7 spectral wavebands centred at 405, 450, 470, 530, 620, 660, or 730 nm and under 250 μM or 2.5 μM $[\text{O}_2]$. Culture tubes were closed with an inert silicone stopper perforated by an aeration input tube extending to the bottom of the culture tube, and a pressure outlet tube. We used aeration with a total gas flow rate of around $\sim 140 \text{ mL min}^{-1} \text{ tube}^{-1}$ through a $0.2 \mu\text{m}$ sterile microfilter provided via a G400 gas mixing system (Qubit Systems Inc., Kingston, Ontario, Canada). $\sim 250 \mu\text{M}$ $[\text{O}_2]$ was achieved by sparging with lab air (78% N_2 , 21% O_2 , 1% Ar and 0.05% CO_2). $\sim 2.5 \mu\text{M}$ $[\text{O}_2]$ was achieved by sparging with a gas mixture containing 99.95% N_2 and 0.05% CO_2 . $[\text{O}_2]$ *in situ* was verified using oxygen optodes (PyroScience, Germany) inserted into tubes for real-time measurements (data not presented), with software correction to account for the salinity of the media (8 PSU). The pH of tested cultures remained about 8, with limited fluctuation during the growth experiment (data not presented).

Chlorophyll-specific growth rates

Picocyanobacterial growth was monitored every 5 minutes by automatically recording OD_{680} , OD_{720} , and ΔOD ($\Delta\text{OD} = \text{OD}_{680} - \text{OD}_{720}$) for at least 5 days, independently for each culture tube. The chlorophyll-specific growth rates (μ) were determined by fitting logistic growth curves using a modified Levenberg-Marquardt fitting algorithm (Elzhov et al. 2023) to plots of the

chlorophyll *a* proxy of ΔOD vs. elapsed time (d) for each combination of strain, spectral waveband, and $[O_2]$.

Picocyanobacteria cell counts

Picocyanobacterial cells mL^{-1} were estimated using linear regression models of OD at 680 nm or 720 nm vs. calibration counts of cell suspension densities (cell mL^{-1}) (Table S1). The OD of cultures was measured using MCMIX-OD PSI Multicultivators (Photon Systems Instruments, Drásov, Czech Republic) and cell suspension density measures were conducted using an ImageXpress Pico Digital microscope equipped with CMOS camera and LED+ image autofocus (ImageXpress Pico Automated Cell Imaging System, Molecular Devices, LLC., CA, USA). Culture samples were preserved with 4% glutaraldehyde and kept at $-80^{\circ}C$ until the microscopy measures. Fixed samples of culture ($V = 10 \mu L$) were transferred to surface treated Tissue Culture (TC) black walled 96-well plates (Corning® Falcon® Microplate, MilliporeSigma, Merck, Darmstadt, Germany) with a transparent flat bottom containing $200 \mu L$ of f/2 media and centrifuged using a Beckman J-20 centrifuge with a swinging bucket JS-4.3 rotor at 4500 rpm (Beckman Coulter, Brea, California, United States). Cells were imaged with the Cy5 channels (Excitation: 630/40 nm; Emission: 695/45 nm; Dichroic: 655 nm) using selectable confocal geometries, which differentiates cyanobacterial cells from co-occurring heterotrophic bacteria, and counted using a 63x objective in fluorescence imaging modes. Quantitative analysis on images acquired from automated microscopy obtained from 96-well microplates was performed using the CellReporterXpress Image Acquisition and Analysis Software. The representative cell number mL^{-1} was calculated based on the dilution factor and selected count area from each well (Wlodkowic et al. 2022).

Pigment content and pigment ratio

Whole-cell absorbance spectra of picocyanobacteria cells were collected using an integrating cavity spectrophotometer (CLARITY 17 UV/Vis/NIR, On-Line Instrument Systems, Inc., Bogart, GA, USA) according to the method proposed by Blake and Griff (2012). The sample and reference observation cavities of the spectrophotometer were filled with 8 mL of f/2 medium at salinity 8 PSU. After establishing a baseline absorbance spectra from 375 to 710 nm, 4 mL culture medium was replaced with 4 mL of culture in the sample cavity. Pathlength corrected absorbance per cm was calculated using J avor i coefficients (J avor i et al. 2006). We then conducted estimations of pigment content ($\mu\text{g mL}^{-1}$) including Chlorophyll *a* (Chl *a*), Carotenoids (Car), Phycoerythrin (PE), Phycocyanin (PC), and Allophycocyanin (APC) from the PC-rich and PE-rich *Synechococcus* cultures. These estimations were based on established linear correlations between pigment content, determined through extraction methods (Strickland and Parsons 1972; Bennett and Bogorad 1973), and absorbance values of individual pigment peaks (Car; 480 nm, PE; 565 nm, PC; 620 nm, APC; 650 nm, and Chl *a*; 665 nm) obtained from whole-cell absorbance spectra (Table S2). Additionally, we summed PE, PC, and APC protein to total Phycobiliproteins content.

Using whole-cell absorbance spectra of *Synechococcus* cultures, we also estimated Photosynthetically Usable Radiation (PUR; $\mu\text{mol photons m}^{-2}\text{s}^{-1}$) according to (Morel 1978).

PSII effective absorption cross section of PSII, turnover time of PSII photochemistry, and photochemical quenching

We harvested 4 mL of picocyanobacteria cultures repeatedly across the growth trajectories for photophysiological characterizations. For the low oxygen cultures, to ensure

photophysiological measurements were taken at low O_2 of $\sim 2.5 \mu M$, we bubbled gently with N_2 from a gas cylinder during measurements. $[O_2]$ was verified in culture samples for photophysiological measurements using oxygen optodes (PyroScience, Germany) inserted (data not presented).

We used Fast Repetition & Relaxation chlorophyll fluorescence (FRRf) (Kolber et al. 1998) (Solisense, USA), with a lab built temperature control jacket ($22^\circ C$), to apply a series of 100 excitation flashlets of $1.6 \mu s$ to drive saturation of PSII variable fluorescence, followed immediately by logarithmically spaced flashlets to track relaxation of variable fluorescence. Induction/relaxation trajectories were fit using the onboard Solisense LIFT software (Falkowski and Kolber 1993; Kolber et al. 1998).

We used a double tap protocol (Xu et al. 2017), where FRRf induction/relaxation trajectories were collected during a rapid actinic light curve sequence increasing in steps of 10 s at 0, 20, 40, 80, 160, and $320 \mu mol \text{ photons } m^{-2}s^{-1}$ PAR. We applied 1 s darkness between the sequential 10 s steps of the light response curves, to allow re-opening of PSII immediately after application of the sequential increasing light steps. Flashlets and actinic light were delivered from LED emitters centred at Ex_{445nm} , preferentially exciting chlorophyll; Ex_{470nm} , preferentially exciting phycourobilin (PUB); Ex_{535nm} , preferentially exciting phycoerythrin (PE); or Ex_{590nm} , preferentially exciting phycocyanin (PC). Excitation flashlets and actinic light wavebands were matched for each run. These actinic and excitation wavebands in turn approximated 4 of our 7 growth light wavebands (450, 470, 530 & 620 nm), allowing us to evaluate *in situ* photosynthetic performance for those culture conditions.

Flashlet power delivered to the samples during the $1.6 \mu s$ flashlet duration was adjusted to achieve saturation of variable fluorescence; Ex_{445nm} at $60000 \mu mol \text{ photons } m^{-2}s^{-1}$ PAR; Ex_{470nm}

at 30000 $\mu\text{mol photons m}^{-2}\text{s}^{-1}$ PAR; $\text{Ex}_{535\text{nm}}$ at 25000 $\mu\text{mol photons m}^{-2}\text{s}^{-1}$ PAR; while for $\text{Ex}_{590\text{nm}}$ excitation power at 14000 $\mu\text{mol photons m}^{-2}\text{s}^{-1}$, calibrated using a quantum sensor (LI-250, LI-COR, Inc.) in the temperature controlled cuvette.

We estimated effective absorption cross section of PSII (σ_{PSII} ; $\text{nm}^2 \text{ quanta}^{-1}$); turnover time of PSII photochemistry (τ_{PSII} ; μs); and the photochemical quenching coefficient (q_p) using the FRRf induction curves, following (Xu et al. 2017). We fit a model with three τ_{PSII} to describe the re-opening of PSII after closure by the saturating flash train. For subsequent analyses we estimated an average of the three τ_{PSII} , weighted by their respective amplitudes, to describe the overall time to reopen PSII after closure.

PSII electron flux

We calculated (Eq. (1)) an uncalibrated fluorescence based estimator for volumetric electron transport, JV_{PSII} , ($\text{k} \times \text{e}^- \text{ L}^{-1} \text{ s}^{-1}$) under $\text{Ex}_{445\text{nm}}$, blue; $\text{Ex}_{470\text{nm}}$, blue-green; $\text{Ex}_{535\text{nm}}$, green; or $\text{Ex}_{590\text{nm}}$, red-orange excitation bands (Oxborough et al. 2012; Boatman et al. 2019; Tortell and Suggett 2021).

$$JV_{\text{PSII}} = \frac{\sigma_{\text{PSII}}' \times q_p \times I \times F_O}{\sigma_{\text{PSII}}} \quad (1)$$

where σ_{PSII}' is effective absorption cross section for PSII photochemistry under the relevant actinic PAR step ($\text{nm}^2 \text{ quanta}^{-1}$); q_p is an estimate of the fraction of PSII open for photochemistry estimated according to Oxborough and Baker (1997); I is the applied PAR ($\mu\text{mol photons m}^{-2}\text{s}^{-1}$); F_O is the minimum fluorescence from a given sample and excitation waveband (relative fluorescence) and σ_{PSII} is the maximum effective absorption cross section for PSII photochemistry from a given sample and excitation waveband ($\text{nm}^2 \text{ quanta}^{-1}$).

We calibrated the JV_{PSII} estimator to absolute rates of electron transport (Eq. (2)) using parallel measures of oxygen evolution ($\mu\text{mol O}_2 \text{ L}^{-1} \text{ s}^{-1}$), captured simultaneously with the FRRf measures, taken below light saturation of electron transport to limit distortion from electron fluxes back to oxygen under super-saturating light (Hughes et al. 2018), using a FireSting robust oxygen probe (PyroScience, Germany) inserted in the cuvette for select Rapid Light Curve (RLC) runs (Table S3).

$$JV_{PSII}(e^- \text{ L}^{-1} \text{ s}^{-1}) = \frac{\text{Uncalibrated } JV_{PSII}(e^- \text{ L}^{-1} \text{ s}^{-1})}{\text{Calibration slope}} \quad (2)$$

We converted JV_{PSII} ($\mu\text{mol e}^- \text{ L}^{-1} \text{ s}^{-1}$) to JV_{PSII} ($\mu\text{mol e}^- \mu\text{mol Chl } a^{-1} \text{ d}^{-1}$) by performing Chl *a* ($\mu\text{g L}^{-1}$) measurements using Trilogy Laboratory Fluorometer (Turner Designs, Inc., CA, USA) equipped with Chlorophyll In-Vivo Module, on the samples taken for the FRRf measurements.

To generate an index of the ratio of Chl *a* : PSII we divided PSII electron transport ($e^- \text{ PSII}^{-1} \text{ s}^{-1}$) by JV_{PSII} ($e^- \text{ Chl}^{-1} \text{ s}^{-1}$), both estimated under $\text{Ex}_{445\text{nm}}$, with units cancelling to Chl *a* : PSII. Since the number of Chl *a* directly associated with the core of PSII is fixed, variations in Chl *a* to PSII reflect changes in the PSI:PSII ratio, and possibly the presence of other chl-containing complexes.

Statistical analysis

We used R version 4.3.0 (R Core Team 2023) running under RStudio (Posit team 2022). We performed three-way factorial ANOVA (*aov()* function; R Base package) to determine whether strain, growth waveband, and $[\text{O}_2]$ significantly influence the chlorophyll-specific growth rate ($\mu; \text{d}^{-1}$; Table S4) or pigment content (Table S5). We also performed three-way factorial ANOVA (*aov()* function) to determine whether strain, Actinic PAR, and $[\text{O}_2]$ significantly influence the

responses of σ_{PSII} (Table S6); τ_{PSII} (Table S7); q_p (Table S8); or JV_{PSII} (Table S9) to increasing light. We fit the light response curves of JV_{PSII} with a three parameter model (Harrison and Platt 1986) using (Elzhov et al. 2023) for *nlsLM()* function. Three-way factorial ANOVA (*aov()* function; R Base package) was performed to determine whether strain, growth waveband, and $[\text{O}_2]$ significantly influence Chl *a* to PSII (Table S10).

We used *t*-tests of linear regressions to compare data across different strains and $[\text{O}_2]$ for a given growth waveband, for chlorophyll-specific growth rate vs. Phycobiliproteins to Chl *a* ratio (Table S11). We also performed *t*-tests of linear fits to compare data across different strains and $[\text{O}_2]$ in situations in which cultures were excited by, and growing in, corresponding growth wavebands of 450, 470, 530, or 620 nm, for chlorophyll-specific growth rate vs. JV_{PSII} (Table S12). Statistical differences for all analyses were determined at significance level $\alpha = 0.05$.

The manuscript was prepared as a Rmarkdown document (Handel 2020) with figures plotted using ggplot2 (Wickham 2016) and patchwork (Pedersen 2024) packages. All metadata, data, and code is available on GitHub (<https://github.com/FundyPhytoPhys/BalticO2>).

Results

Chlorophyll-specific growth rates across $[\text{O}_2]$, spectral wavebands, and strains

We used logistic curve fits (Fig. S1) to determine chlorophyll-specific growth rates (μ ; d^{-1}) for PC-rich and PE-rich cultures of *Synechococcus* grown under spectral wavebands centred at 405, 450, 470, 530, 620, 660, or 730 nm, and $[\text{O}_2]$ of 250 μM or 2.5 μM (Fig. 1). Growth curves, tracked as OD_{680} , OD_{720} , ΔOD and logistic fits of ΔOD vs. elapsed time are shown in Fig. S1 in Supplementary materials. Cell-specific growth rates (μ) were also determined using OD_{720} (Fig. S2). Strain, growth waveband, $[\text{O}_2]$, and their interactions, significantly affected μ (Table S4).

251 PC-rich and PE-rich *Synechococcus* grow under 2.5 μM $[\text{O}_2]$, across the range of tested
252 spectral wavebands from 405 – 730 nm. In contrast, under 250 μM $[\text{O}_2]$, the PC-rich strain failed
253 to grow under 405 nm, while the PE-rich strain failed to grow under 405, 450, and 730 nm. The
254 PC-rich strain showed generally similar growth rates under 2.5 and 250 μM $[\text{O}_2]$, across tested
255 spectral wavebands (nm). In contrast the PE-rich strain achieved faster growth rates under 2.5 μM
256 $[\text{O}_2]$ than under 250 μM $[\text{O}_2]$.

257 PC-rich *Synechococcus* showed a peak in growth rate under both $[\text{O}_2]$ and red light of 620
258 or 660 nm, absorbed by phycocyanin and chlorophyll. Under 2.5 μM $[\text{O}_2]$ the PE-rich strain
259 showed high growth rates under 530 nm – 660 nm absorbed by phycoerythrin, phycocyanin, and
260 chlorophyll; while under 250 μM $[\text{O}_2]$, the PE-rich strain showed the highest growth rate under
261 green light of 530 nm absorbed by phycoerythrin.

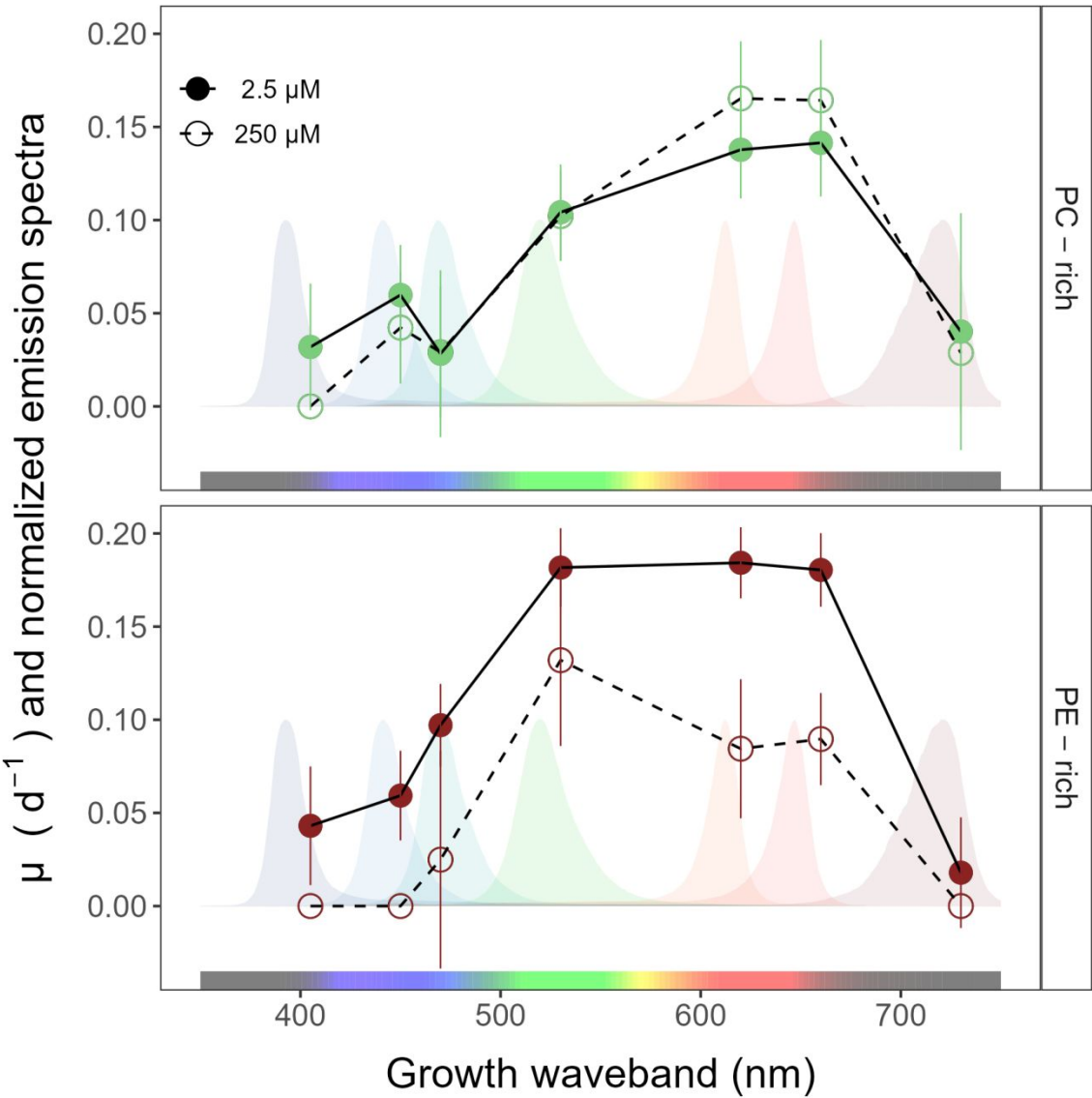


Fig. 1: Chlorophyll-specific growth rates (μ ; d^{-1}) vs. growth waveband (nm, shaded regions). Growth rates (\pm SE) were estimated from logistic fits of chlorophyll proxy $\text{OD}_{680} - \text{OD}_{720}$ (ΔOD) vs. elapsed time (Fig. S1), for PC-rich (green circle) and PE-rich (red circle) cultures of *Synechococcus* grown at spectral wavebands of 405, 450, 470, 530, 620, 660, or 730 nm, and $[\text{O}_2]$ of 250 μM (open symbols and dashed line) or 2.5 μM (closed symbols and solid line).

Pigment content and pigment ratio across [O₂], spectral wavebands, and strains

Fig. 2a presents Chlorophyll *a* (Chl *a*), Phycobiliproteins (Phyco), or Carotenoids (Car) content (pg cell⁻¹) vs. growth waveband (nm) for PC-rich and PE-rich cultures of *Synechococcus* grown at spectral wavebands centred at 405, 450, 470, 530, 620, 660, or 730 nm and 250 or 2.5 μM [O₂]. We also calculated the Car to Chl *a* ratio, and the ratio of the sum of Phycobiliproteins to Chl *a* (μg:μg) for each strain (Fig. S3). Moreover, phycobiliproteins:Chlorophyll *a* ratio (μg:μg) and chlorophyll-specific growth rates (μ; d⁻¹) vs. Photosynthetically Usable Radiation (PUR, μmol photons m⁻²s⁻¹) for PC-rich and PE-rich cultures of *Synechococcus* grown at spectral wavebands of 405, 450, 470, 530, 620, 660, or 730 nm and 250 μM [O₂] or 2.5 μM [O₂] are presented in Fig. S4.

To focus on the responses of growing cells, we omit pigmentation data from those PE-rich cultures which showed negligible growth under 405, 450, 730 nm and 250 μM [O₂]; and from those PC-rich cultures which showed negligible growth under 405 nm and 250 μM [O₂].

Strain, growth waveband, [O₂], and their interactions, significantly affected cell-specific Chl *a*, Phycobiliproteins, and Car content (Table S5). For the PC-rich strain, the highest Chl *a*, Phycobiliproteins, and Car contents were recorded after growth under 730 nm. The phycobiliproteins content was higher under 250 μM [O₂] than under 2.5 μM [O₂] for the PC-rich strain. In contrast, for PE-rich *Synechococcus*, phycobiliproteins content was significantly lower under 250 μM [O₂] than under 2.5 μM [O₂], with the highest phycobiliproteins content under 620 nm and 2.5 μM [O₂].

Chlorophyll-specific growth rates (μ; d⁻¹) show positive linear responses to the Phycobiliproteins:Chlorophyll *a* ratio (μg:μg), for both PC-rich and PE-rich *Synechococcus* (Fig. 2b), although the relations vary across strain and [O₂] (Table S11).

293

Draft

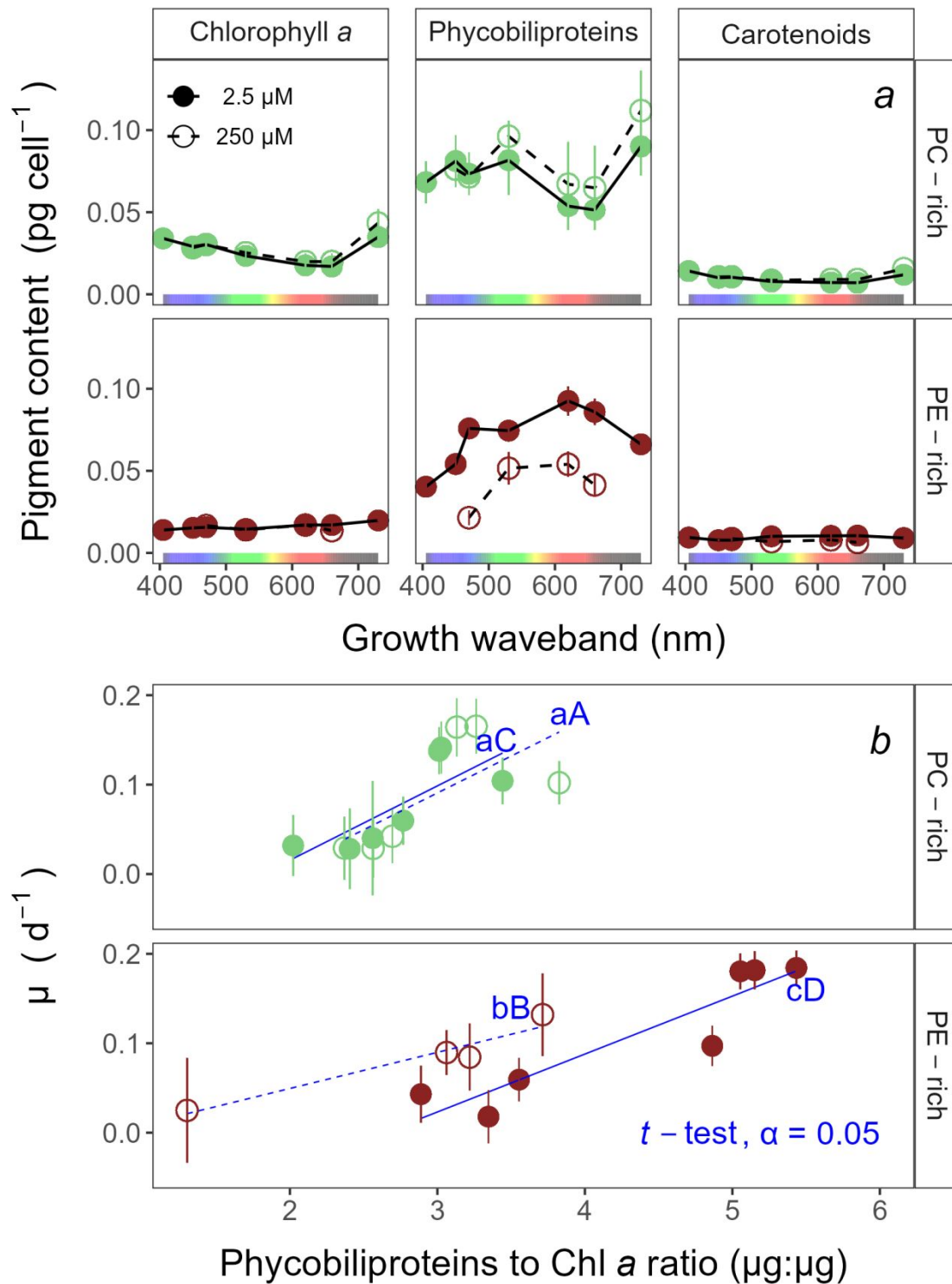


Fig. 2: Pigment content (pg cell⁻¹) vs. growth waveband (nm) (a) and Chlorophyll-specific growth rates (μ ; d⁻¹) vs. Phycobiliproteins:Chlorophyll *a* ratio ($\mu\text{g}:\mu\text{g}$) (b) for PC-rich (green circle) and

PE-rich (red circle) cultures of *Synechococcus* grown at spectral wavebands of 405, 450, 470, 530, 620, 660, or 730 nm and 250 μM $[\text{O}_2]$ (open symbols and dashed line) or 2.5 μM $[\text{O}_2]$ (closed symbols and solid line). Data not presented for those PE-rich cultures which showed negligible growth under 405, 450, 730 nm and 250 μM $[\text{O}_2]$; nor for those PC-rich cultures which showed negligible growth under 405 nm and 250 μM $[\text{O}_2]$. Blue lines show linear model fit for data from each strain and $[\text{O}_2]$ (solid for 2.5 μM $[\text{O}_2]$ or dashed for 250 μM $[\text{O}_2]$) across spectral wavebands. Different blue lowercase letters indicate statistically significant differences between the fit models for different $[\text{O}_2]$ within a given strain. Different blue uppercase letters indicate statistically significant differences between the fit models for different strains within a given $[\text{O}_2]$ (t -test; $p < 0.05$).

Effective absorption cross sections, turnover times, and photochemical quenching of PSII across $[\text{O}_2]$, spectral wavebands, and strains

Light response curves of effective absorption cross section of PSII (σ_{PSII} ; $\text{nm}^2 \text{ quanta}^{-1}$); turnover time of PSII photochemistry (τ_{PSII} ; μs); and the photochemical quenching coefficient (q_p) vs. Actinic PAR ($\mu\text{mol photons m}^{-2}\text{s}^{-1}$) (Fig. 3a-c) are shown for PC-rich and PE-rich cultures grown in, and excited by, corresponding wavebands of 450, 470, 530, or 620 nm, at 250 μM or 2.5 μM $[\text{O}_2]$. We omit functional data determined for those PE-rich cultures which showed negligible growth under 405, 450, 730 nm and 250 μM O_2 ; and for those PC-rich cultures which showed negligible growth under 405 nm and 250 μM O_2 . In the Supplementary materials (Fig S5-S7), we also show the light response curves for all available excitation ($\text{Ex}_{445\text{nm}}$, blue; $\text{Ex}_{470\text{nm}}$, blue-green; $\text{Ex}_{535\text{nm}}$, green; or $\text{Ex}_{590\text{nm}}$, orange) and growth waveband (450, 470, 530, or 620 nm) cross-combinations.

σ_{PSII} (Fig. 3a), a measure of excitation driving PSII photochemistry, was low and shows little change with increasing actinic light during excitation through chlorophyll at $\text{Ex}_{445\text{nm}}$. For the PC-rich strain, under orange excitation at $\text{Ex}_{590\text{nm}}$, σ_{PSII} showed an initial small increase from darkness to the growth light level, followed by a mild decrease with increasing Actinic PAR, and was higher at $250 \mu\text{M} [\text{O}_2]$ compared to $2.5 \mu\text{M} [\text{O}_2]$. For the PE-rich strain, we again see a small increase from darkness to the growth light level, followed by a decrease in σ_{PSII} with increasing Actinic PAR. Moreover, for the PE-rich strain σ_{PSII} was higher in low $[\text{O}_2]$ conditions than in high $[\text{O}_2]$ conditions. Strain, Actinic PAR, and $[\text{O}_2]$ significantly influenced σ_{PSII} under excitation at $\text{Ex}_{590\text{nm}}$ (Table S6).

For the PC-rich strain, across the excitation wavebands tested, τ_{PSII} showed an acceleration (decrease) from darkness to growth light Actinic PAR (Fig. 3b), to a plateau of $\sim 800 \mu\text{s}$. PE-rich strains, on the other hand, showed a progressive acceleration (decrease) with increasing Actinic PAR under excitation at $\text{Ex}_{470\text{nm}}$, $\text{Ex}_{535\text{nm}}$, or $\text{Ex}_{590\text{nm}}$, declining towards $\sim 400 \mu\text{s}$ under $\text{Ex}_{590\text{nm}}$. Thus, the PE-rich strain showed more capacity to remove electrons from PSII. τ_{PSII} was generally faster (smaller) for both PC-rich and PE-rich strains under $250 \mu\text{M} [\text{O}_2]$. Strain, Actinic PAR, and $[\text{O}_2]$ significantly affected τ_{PSII} at $\text{Ex}_{470\text{nm}}$, $\text{Ex}_{535\text{nm}}$ and $\text{Ex}_{590\text{nm}}$ (Table S7).

q_p , a measure of the fraction of PSII available for photochemistry, showed a strong decrease with increasing Actinic PAR across the excitation wavebands tested (Fig. 3c). q_p generally remained higher for both PC-rich and PE-rich strains under $250 \mu\text{M} [\text{O}_2]$. Strain, Actinic PAR, and $[\text{O}_2]$ significantly affected q_p at $\text{Ex}_{470\text{nm}}$, $\text{Ex}_{535\text{nm}}$, and $\text{Ex}_{590\text{nm}}$ (Table S8).

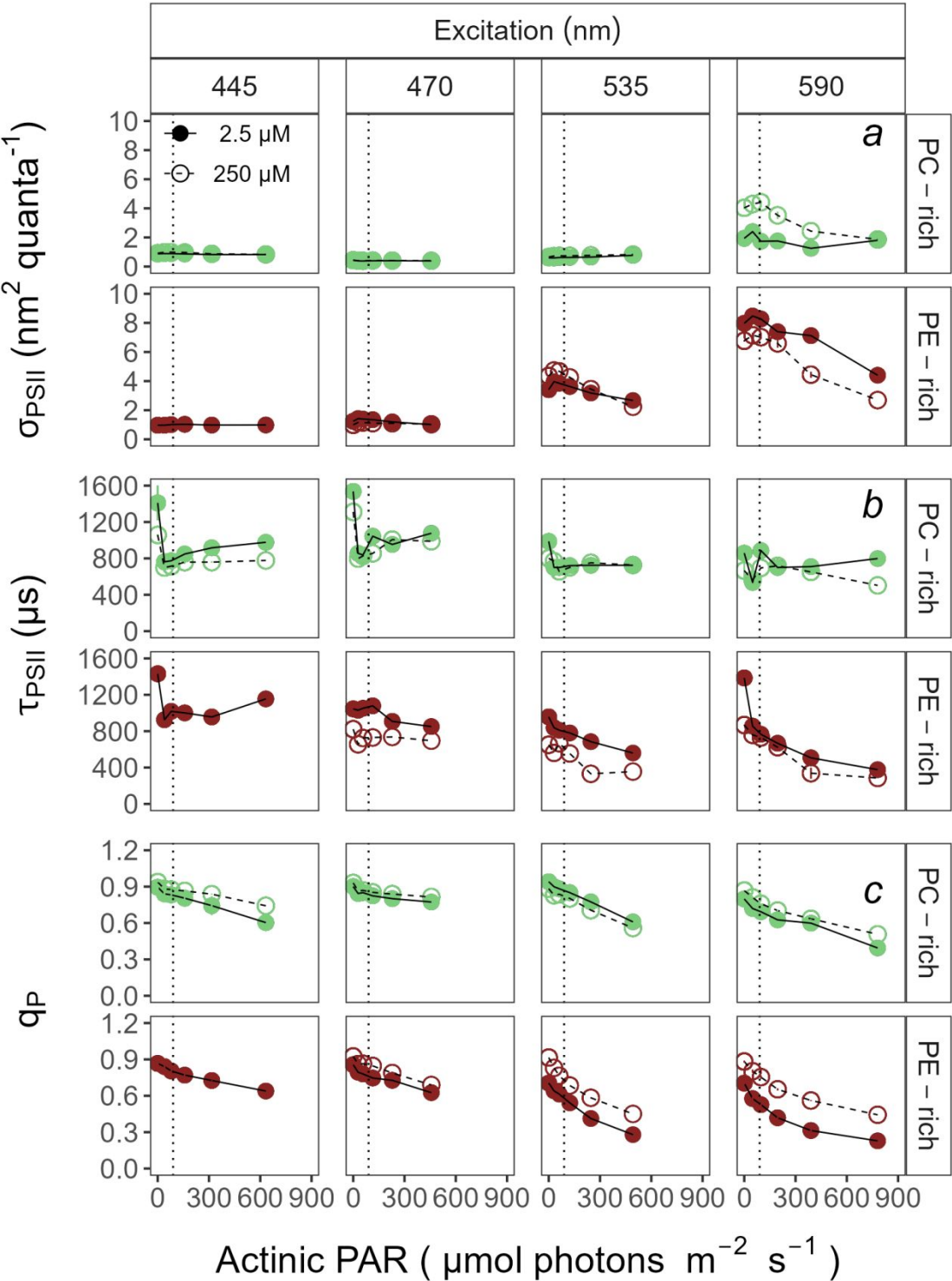


Fig. 3: Effective absorption cross section of PSII (σ_{PSII} ; $\text{nm}^2 \text{ quanta}^{-1}$) (a); turnover time of PSII photochemistry (τ_{PSII} ; μs) (b); or photochemical quenching coefficient (q_p) (c) vs. Actinic PAR

($\mu\text{mol photons m}^{-2}\text{s}^{-1}$). Parameters were estimated using FRRf induction curves with excitation (columns) at $\text{Ex}_{445\text{nm}}$, blue; $\text{Ex}_{470\text{nm}}$, blue-green; $\text{Ex}_{535\text{nm}}$, green; or $\text{Ex}_{590\text{nm}}$, orange; for PC-rich (green circle) or PE-rich (red circle) cultures of *Synechococcus*. Data show situations in which cultures were excited by, and growing in, corresponding growth wavebands of 450, 470, 530, or 620 nm and 250 μM $[\text{O}_2]$ (open symbols and dashed line) or 2.5 μM $[\text{O}_2]$ (closed symbols and solid line). The vertical lines show half diel peak PAR growth light of 90 $\mu\text{mol photons m}^{-2}\text{s}^{-1}$. Data not presented for those PE-rich cultures which showed negligible growth under 405, 450, 730 nm and 250 μM $[\text{O}_2]$; nor for those PC-rich cultures which showed negligible growth under 405 nm and 250 μM $[\text{O}_2]$.

PSII electron flux across $[\text{O}_2]$, spectral wavebands, and strains

PSII electron flux (JV_{PSII}) measures the generation of reductant available to support biosynthetic assimilation and growth. JV_{PSII} was estimated using FRRf inductions with excitation at $\text{Ex}_{445\text{nm}}$, $\text{Ex}_{470\text{nm}}$, $\text{Ex}_{535\text{nm}}$, or $\text{Ex}_{590\text{nm}}$, corresponding to growth wavebands of 450, 470, 530, or 620 nm and 250 μM or 2.5 μM $[\text{O}_2]$. To focus on responses of growing cells, we do not present JV_{PSII} data for those PE-rich cultures which showed negligible growth under 405, 450, 730 nm and 250 μM O_2 ; nor for those PC-rich cultures which showed negligible growth under 405 nm and 250 μM O_2 . PSII electron flux (JV_{PSII} ; $\mu\text{mol e}^- \mu\text{mol Chl } a^{-1} \text{ s}^{-1}$) vs. Actinic PAR ($\mu\text{mol photons m}^{-2}\text{s}^{-1}$) estimated using FRRf induction curves with excitation at $\text{Ex}_{445\text{nm}}$, blue; $\text{Ex}_{470\text{nm}}$, blue-green; $\text{Ex}_{535\text{nm}}$, green; or $\text{Ex}_{590\text{nm}}$, orange; for PC-rich or PE-rich cultures of *Synechococcus* grown at spectral bandwidths of 450, 470, 530, or 620 nm and O_2 concentrations of 250 μM or 2.5 μM are also presented (Fig. S8).

Light response curves of PSII electron flux (JV_{PSII} ; $\mu\text{mol e}^- \mu\text{mol Chl } a^{-1} \text{ s}^{-1}$) vs. Actinic PAR ($\mu\text{mol photons m}^{-2}\text{s}^{-1}$) are shown in Fig. 4a. For the PC-rich strain, under all tested excitations ($\text{Ex}_{445\text{nm}}$, $\text{Ex}_{470\text{nm}}$, $\text{Ex}_{535\text{nm}}$, or $\text{Ex}_{590\text{nm}}$), JV_{PSII} increased with increasing Actinic PAR, and did not fully saturate across the range of tested actinic PAR. Under all excitations, except $\text{Ex}_{590\text{nm}}$, JV_{PSII} was higher at 2.5 μM $[\text{O}_2]$ compared to 250 μM $[\text{O}_2]$ for the PC-rich strain. Conversely, for the PE-rich strain, JV_{PSII} under $\text{Ex}_{470\text{nm}}$, $\text{Ex}_{535\text{nm}}$, or $\text{Ex}_{590\text{nm}}$ was higher at 250 μM $[\text{O}_2]$ compared to 2.5 μM $[\text{O}_2]$. Moreover, for the PE-rich strain, JV_{PSII} plateaued above $\sim 90 \mu\text{mol photons m}^{-2}\text{s}^{-1}$ under $\text{Ex}_{535\text{nm}}$, or $\text{Ex}_{590\text{nm}}$ for both low and high $[\text{O}_2]$. Strain, Actinic PAR, and $[\text{O}_2]$ significantly influence JV_{PSII} under some of the tested excitations (Table S9), but JV_{PSII} for cultures grown under, and excited through, $\text{Ex}_{445\text{nm}}$, absorbed by chlorophyll, shows no difference between low and high $[\text{O}_2]$ with increasing actinic light.

Fig. 4b presents linear regressions between chlorophyll-specific growth rates (μ ; d^{-1}) and cumulative diel PSII electron flux (JV_{PSII} ; $\mu\text{mol e}^- \mu\text{mol Chl } a^{-1} \text{ d}^{-1}$) measured under half ($90 \mu\text{mol photons m}^{-2}\text{s}^{-1}$) of the diel peak PAR growth light. μ (d^{-1}), as expected, was positively correlated with JV_{PSII} , with slopes significantly greater than 0. $[\text{O}_2]$ significantly influences the linear regressions between chlorophyll-specific growth rates and PSII electron flux for both PC-rich and PE-rich strains of *Synechococcus* ($p < 0.05$, Table S12). In the PC-rich strain higher $[\text{O}_2]$ increases the growth yield of electron transport. In contrast, the PE-rich strain, under higher $[\text{O}_2]$, decreases the growth yield of electron transport. However, the regressions for a given $[\text{O}_2]$ are not significantly different between the two strains ($p > 0.05$, Table S12).

Strain, actinic PAR waveband, and $[\text{O}_2]$ significantly influence Strain, Actinic PAR, and $[\text{O}_2]$ significantly influence our metric of Chl a : PSII (Fig. S9, Table S10), with Chl a : PSII higher

388 under 250 than under 2.5 μM $[\text{O}_2]$ in the PC-rich strain, and Chl a : PSII generally lower in the
389 PC-rich stain compared to the PE-rich strain.

390

Draft

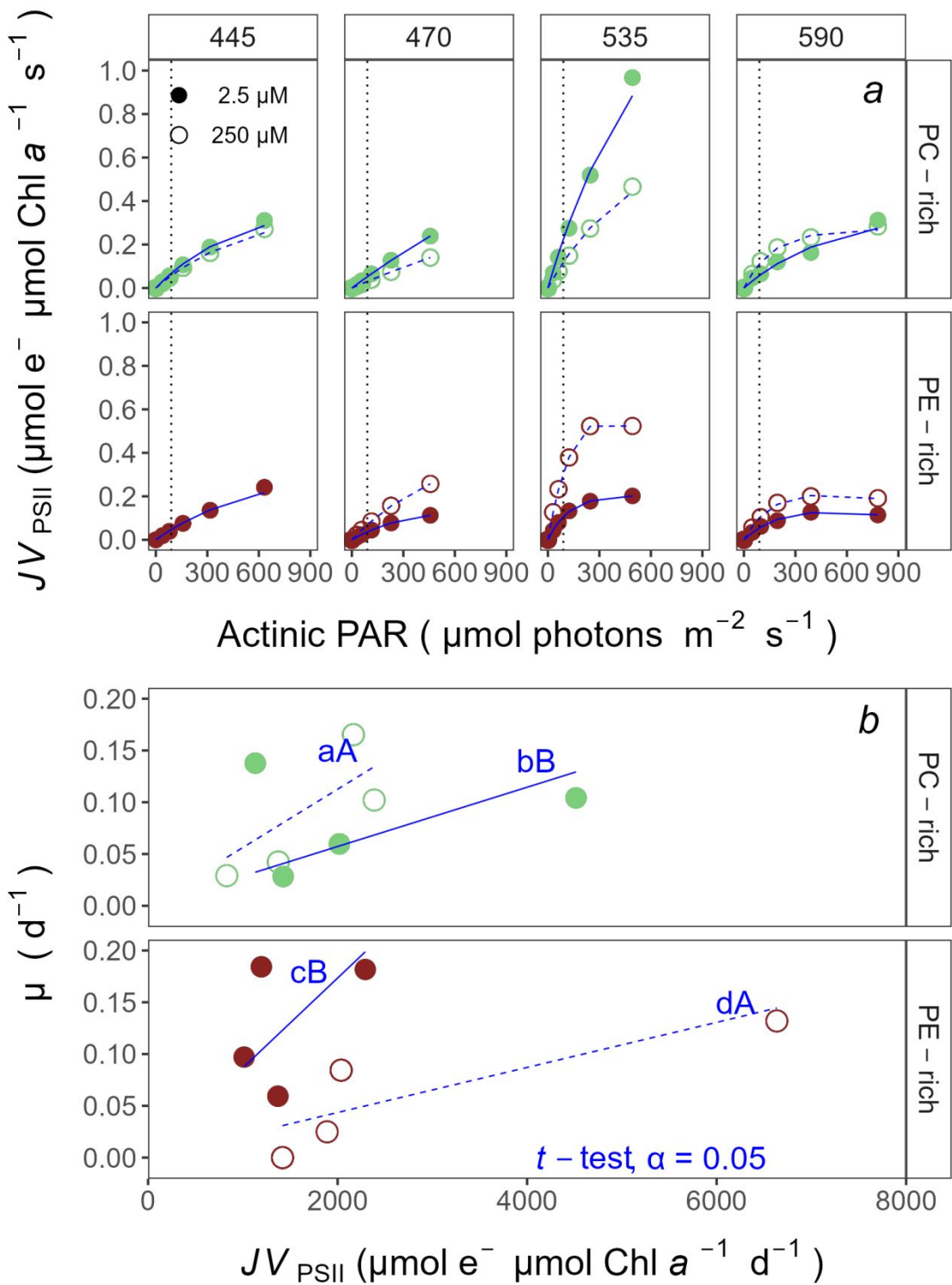


Fig. 4: PSII electron flux (JV_{PSII} ; $\mu\text{mol e}^- \mu\text{mol Chl } a^{-1} \text{ s}^{-1}$) vs. Actinic PAR ($\mu\text{mol photons m}^{-2} \text{ s}^{-1}$)

(a). JV_{PSII} was estimated using FRRf induction curves with excitation at $\text{Ex}_{445\text{nm}}$, blue; $\text{Ex}_{470\text{nm}}$,

blue-green; Ex_{535nm}, green; or Ex_{590nm}, orange; for PC-rich (green circle) or PE-rich (red circle) cultures of *Synechococcus*. Data show situations in which cultures were excited by, and growing in, corresponding growth wavebands of 450, 470, 530, or 620 nm and 250 μM [O₂] (open symbols and dashed line) or 2.5 μM [O₂] (closed symbols and solid line). JV_{PSII} vs. Actinic PAR ($\mu\text{mol photons m}^{-2}\text{s}^{-1}$) was fit with a Harrison and Platt Light Response Curve model (Harrison and Platt 1986), used to estimate JV_{PSII} at 90 $\mu\text{mol photons m}^{-2}\text{s}^{-1}$ (vertical dotted lines). Chlorophyll-specific growth rates ($\mu; \text{d}^{-1}$) vs. PSII electron flux ($JV_{\text{PSII}}; \mu\text{mol e}^{-} \mu\text{mol Chl } a^{-1} \text{d}^{-1}$) measured under half (90 $\mu\text{mol photons m}^{-2}\text{s}^{-1}$) of diel peak PAR growth light (*b*). Blue lines (solid for 2.5 μM [O₂] or dashed for 250 μM O₂) show linear model fit for data from each strain across spectral wavebands. Different blue lowercase letters indicate statistically significant differences between the fit models for different [O₂] within a given strain. Different blue uppercase letters indicate statistically significant differences between the fit models for different strains within a given [O₂] (*t*-test; $p < 0.05$).

Discussion

Growth responses of PC-rich and PE-rich picocyanobacteria across [O₂] and spectral wavebands

Picocyanobacteria from the genus *Synechococcus* are major contributors to primary marine production, across a wide range of environments (Śliwińska-Wilczewska et al. 2018a; Aguilera et al. 2023) but interactive influences of [O₂] and spectral wavebands on their growth rates and ecophysiology have not yet been investigated.

PC-rich and PE-rich *Synechococcus* from coastal habitats are exposed to changes in irradiance, spectral waveband, and sometimes [O₂], by vertical movements through the mixed

layer. Fluctuation in spectral wavebands changes the balance between productive photosynthesis, and photoinactivation of PSII (Six et al. 2007), increasing the cost of growth by diverting protein metabolism towards PSII repair (Murphy et al. 2017). Indeed, under 250 μM $[\text{O}_2]$, the PC-rich strain failed to grow under 405 nm, while the PE-rich strain failed to grow under 405 and 450, consistent with accelerated photoinactivation of PSII under blue wavebands (Murphy et al. 2017). In contrast, growth persisted in both strains at 405 & 450 nm under 2.5 μM $[\text{O}_2]$, likely because generation of toxic Reactive Oxygen Species (ROS) was suppressed, lowering the burden of photoinactivation of PSII.

μ shows positive responses to both Phycobiliproteins:Chlorophyll *a* ratio, an index of light capture capacity, and to cumulative diel PSII electron flux (JV_{PSII}) for *Synechococcus*, although the relations varied across strain and with $[\text{O}_2]$. In the PC-rich strain lower $[\text{O}_2]$ lowered the yield of growth per electron flux, while in the PE-rich strain the yield of growth per electron flux increased under lower $[\text{O}_2]$. Note that these regressions excluded those conditions where no growth occurred. In contrast, growth showed no correlation to estimated Photosynthetically Usable Radiation (PUR) (Fig. S4), likely because of variable allocations of excitation from phycobilisomes across growth conditions (Campbell 1996), not captured in the PUR metric based upon light absorption.

Wong et al. (2023) found that vertical structures of phytoplankton communities in OMZ are not sufficiently explained by top-down predation pressure nor light and/or nutrient limitation and thus, some phytoplankton may have a higher than expected direct O_2 requirement, with growth inhibited by low O_2 levels. However, in our work we show that low oxygen levels either do not suppress, and sometimes even benefit, growth of strains representing different *Synechococcus* pigment phenotypes across spectral wavebands. What is more, historical data link major extinction

events to warm climates and oxygen-deficient oceans, with current anthropogenic activities possibly leading to widespread OMZ within a thousand years (Breitburg et al. 2018). The PC-rich *Synechococcus* strain showed generally similar growth rates under high and low tested $[O_2]$, while the PE-rich strain achieved faster growth rates under low (2.5 μM) than under high (250 μM) $[O_2]$. PE-rich *Synechococcus* are typically found at greater depths, and lower light, than are PC-rich strains (Haverkamp et al. 2009; Śliwińska-Wilczewska et al. 2018a) but we suggest that at least some PE-rich strains may actually be limited to lower light niches by the interactions between light level, spectral band, and full air-saturated $[O_2]$. In lower oxygen waters some PE-rich strains may exploit higher light niches nearer the surface.

Physiological adaptations of PC-rich and PE-rich picocyanobacteria to $[O_2]$ and spectral wavebands

Synechococcus strains vary widely in pigment composition, enabling them to exploit different spectral niches (Moore et al. 1995; Six et al. 2007; Grébert et al. 2018; Efimova et al. 2020). With a small diameter of 0.8–2.0 μm , *Synechococcus* possess a high surface-to-volume ratio (Śliwińska-Wilczewska et al. 2018b), minimizing pigment package effects (Finkel 2001), and resulting in high optical absorption per pigment. This characteristic allows them to thrive under low light deep in the water column (Moore et al. 1995), and to disproportionately influence subsurface light fields (Berthold and Schumann 2020). Although limited package effect increases photon capture per pigment investment, it also increases *Synechococcus* susceptibility to light-induced damage (Llabrés and Agustí 2006, 2010). In some *Synechococcus*, a carotenoid-protein complex regulates the connectivity of the phycobilisome to the reaction center, mediating a form of non-photochemical quenching of excitation (Wilson et al. 2006; Gorbunov et al. 2011;

Kirilovsky 2015). In our work we found no change in bulk carotenoids content (Fig. 2), nor in Car to Chl *a* ratio (Fig. S3) under the different [O₂]. What is more, for the chosen PE-rich strain, the carotenoids content did not change across tested wavebands. On the other hand, for the chosen PC-rich strain, a slight increase in carotenoids content was recorded under 405 nm, although these cells were not growing and were thus under stress.

σ_{PSII} was low and showed little change with increasing actinic light during excitation through chlorophyll at Ex_{445nm}, because in cyanobacteria the number of chlorophyll per PSII is low, and nearly fixed, so the effective absorption cross section of PSII for chlorophyll is low (Xu et al. 2018). With excitation through the phycobilisomes at 535 and 590 nm σ_{PSII} rose to a peak near the acclimated light level of $\sim 90 \mu\text{mol photons m}^{-2}\text{s}^{-1}$ (Campbell and Oquist 1996), reflecting the state transition from State II in the dark towards State I near the growth light level, with subsequent decrease in σ_{PSII} , as excitation is again directed away from PSII.

τ_{PSII} was generally faster for both the chosen PC-rich and PE-rich strains under 250 μM [O₂], consistent with the cyanobacterial capacity for pseudo-cyclic electron flows away from PSII to [O₂] (Campbell et al. 1999; Grossman et al. 2010; Allahverdiyeva et al. 2015; Hughes et al. 2018), thereby controlling feedback inhibition of electron transport. In parallel, q_{P} was generally higher for the PC-rich, and particularly for the PE-rich strain, under 250 μM [O₂], since cyanobacteria show strong capacity for electron flow away from PSII to O₂ (Campbell et al. 1999; Hughes et al. 2018), particularly under excess excitation above the acclimated PAR of $\sim 90 \mu\text{mol photons m}^{-2}\text{s}^{-1}$. In spite of this faster electron transport performance under 250 μM [O₂] the PE-rich strain grew faster under 2.5 μM [O₂], showing an increase in the growth return upon electron transport, possibly because of a decrease in metabolic burden, through suppression of ROS formation under

lower [O₂]. Future genomic comparisons may uncover the bases for these distinct strain responses to changing [O₂].

Picocyanobacteria numerically dominate vast tracts of the oceans, contributing significant primary production, particularly in oligotrophic regions, but also some coastal habitats (Haverkamp 2008; Larsson et al. 2014; Doré et al. 2022; Aguilera et al. 2023). The ecological success of picoplanktonic *Synechococcus* reflects specific lineages occupying different niches to populate the world's oceans (Scanlan 2012). Picocyanobacteria species can share the light spectrum by specializing in different wavelengths (Stomp et al. 2004, 2007; Haverkamp et al. 2009). Competition models and laboratory experiments show that PE-rich picocyanobacteria outperform competitors in green light while PC-rich picocyanobacteria dominate in red light, while both species can coexist across the full spectrum (Stomp et al. 2004, 2007). We now find that spectral wavebands interact with [O₂] as determinants of growth rates across PE- and PC-rich strains of *Synechococcus*, and that changing ocean [O₂] might drive strains of different pigmentation phenotypes into changing ecological niches.

Acknowledgements

We would like to express our sincere gratitude to the Editor, and two Reviewers for their efforts reviewing and improving this manuscript. We thank Naaman M. Omar for assistance with coding, data analyses and culture maintenance; Miranda Corkum who maintained cultures and trained personnel in culture handling; Laurel Genge, and Carlie Barnhill (Mount Allison students) who assisted with R code.

Article information

Data availability statement

Data supporting this study is available on: <https://github.com/FundyPhytoPhys/BalticO2> (public GitHub Repository) and https://docs.google.com/spreadsheets/d/1ZXpwR7Gfto-uRzVdXzMpQF4frbrvMLH_IyLqonFZRSw/edit#gid=0 (URL for MetaDataCatalog).

Code to perform data processing and analyses is available at <https://github.com/FundyPhytoPhys/BalticO2>.

Author information

Author ORCIDs

Sylwia Śliwińska-Wilczewska <https://orcid.org/0000-0002-3147-6605> Mireille Savoie <https://orcid.org/0009-0009-9499-6657> Douglas A. Campbell <https://orcid.org/0000-0001-8996-5463>

Author contributions

Conceptualization: SSW, DAC Data curation: SSW Formal analysis: SSW, MS, DAC Funding acquisition: DAC Investigation: SSW Methodology: SSW, MS, DAC Project administration: DAC Resources: DAC Supervision: DAC Validation: SSW, MS, DAC Visualization: SSW Writing – original draft: SSW, MS, DAC

Competing interests

The authors declare there are no competing interests.

Funding information

This work was supported by Canada Research Chair in Phytoplankton Ecophysiology (DAC) and Latitude & Light; NSERC of Canada Discovery Grant (DAC).

Supplementary material

Supplementary data are available with the article at <https://github.com/FundyPhytoPhys/BalticO2>.

References

- Aguilera, A., Alegria Zufia, J., Bas Conn, L., Gurlit, L., Śliwińska-Wilczewska, S., Budzałek, G., Lundin, D., Pinhassi, J., Legrand, C., and Farnelid, H. 2023. Ecophysiological analysis reveals distinct environmental preferences in closely related Baltic Sea picocyanobacteria. *Environmental Microbiology* **25**(9): 1674–1695. doi:10.1111/1462-2920.16384.
- Allahverdiyeva, Y., Isojärvi, J., Zhang, P., and Aro, E.-M. 2015. Cyanobacterial Oxygenic Photosynthesis is Protected by Flavodiiron Proteins. *Life* **5**(1): 716–743. Multidisciplinary Digital Publishing Institute. doi:10.3390/life5010716.
- Andersson, B., Salter, A.H., Virgin, I., Vass, I., and Styring, S. 1992. Photodamage to photosystem II - primary and secondary events. *Journal of Photochemistry and Photobiology B: Biology* **15**(1): 15–31. doi:10.1016/1011-1344(92)87003-R.
- Bagby, S.C., and Chisholm, S.W. 2015. Response of *Prochlorococcus* to varying CO₂:O₂ ratios. *The ISME Journal* **9**(10): 2232–2245. doi:10.1038/ismej.2015.36.

- 551 Bennett, A., and Bogorad, L. 1973. Complementary Chromatic Adaptation in a filamentous blue-
552 green alga. *Journal of Cell Biology* **58**(2): 419–435. doi:10.1083/jcb.58.2.419.
- 553 Berthold, M., and Schumann, R. 2020. Phosphorus Dynamics in a Eutrophic Lagoon: Uptake and
554 Utilization of Nutrient Pulses by Phytoplankton. *Frontiers in Marine Science* **7**. Frontiers.
555 doi:10.3389/fmars.2020.00281.
- 556 Blake, R., and Griff, M. 2012. In situ spectroscopy on intact *Leptospirillum Ferrooxidans* reveals
557 that reduced cytochrome 579 is an obligatory intermediate in the aerobic iron respiratory chain.
558 *Frontiers in Microbiology* **3**. [accessed 13 June 2023].
- 559 Boatman, T.G., Geider, R.J., and Oxborough, K. 2019. Improving the accuracy of Single Turnover
560 Active Fluorometry (STAF) for the estimation of Phytoplankton Primary Productivity (PhytoPP).
561 *Frontiers in Marine Science* **6**. Frontiers. doi:10.3389/fmars.2019.00319.
- 562 Breitburg, D., Levin, L.A., Oschlies, A., Grégoire, M., Chavez, F.P., Conley, D.J., Garçon, V.,
563 Gilbert, D., Gutiérrez, D., Isensee, K., Jacinto, G.S., Limburg, K.E., Montes, I., Naqvi, S.W.A.,
564 Pitcher, G.C., Rabalais, N.N., Roman, M.R., Rose, K.A., Seibel, B.A., Telszewski, M., Yasuhara,
565 M., and Zhang, J. 2018. Declining oxygen in the global ocean and coastal waters. *Science*
566 **359**(6371): eaam7240. American Association for the Advancement of Science.
567 doi:10.1126/science.aam7240.
- 568 Callieri, C., Cabello-Yeves, P.J., and Bertoni, F. 2022. The “Dark Side” of Picocyanobacteria: Life
569 as We Do Not Know It (Yet). *Microorganisms* **10**(3): 546. Multidisciplinary Digital Publishing
570 Institute. doi:10.3390/microorganisms10030546.

- 571 Campbell, D. 1996. Complementary chromatic adaptation alters photosynthetic strategies in the
572 cyanobacterium *Calothrix*. *Microbiology* **142**(5): 1255–1263. Microbiology Society,.
573 doi:10.1099/13500872-142-5-1255.
- 574 Campbell, D., Clarke, A.K., Gustafsson, P., and Öquist, G. 1999. Oxygen-dependent electron flow
575 influences photosystem II function and *psbA* gene expression in the cyanobacterium
576 *Synechococcus* sp. PCC 7942. *Physiologia Plantarum* **105**(4): 746–755. doi:10.1034/j.1399-
577 3054.1999.105420.x.
- 578 Campbell, D., and Oquist, G. 1996. Predicting Light Acclimation in Cyanobacteria from
579 Nonphotochemical Quenching of Photosystem II Fluorescence, Which Reflects State Transitions
580 in These Organisms. *Plant Physiology* **111**(4): 1293–1298. doi:10.1104/pp.111.4.1293.
- 581 Doré, H., Leconte, J., Guyet, U., Breton, S., Farrant, G.K., Demory, D., Ratin, M., Hoebeke, M.,
582 Corre, E., Pitt, F.D., Ostrowski, M., Scanlan, D.J., Partensky, F., Six, C., and Garczarek, L. 2022.
583 Global Phylogeography of Marine *Synechococcus* in Coastal Areas Reveals Strong Community
584 Shifts. *mSystems* **7**(6): e00656–22. American Society for Microbiology.
585 doi:10.1128/msystems.00656-22.
- 586 Efimova, T.V., Churilova, T.Ya., and Mukhanov, V.S. 2020. The Influence of Light of Different
587 Spectral Qualities on the Photosynthetic Characteristics of C-Phycocyanine-Containing
588 Cyanobacteria *Synechococcus* sp. WH5701. *Russian Journal of Marine Biology* **46**(2): 105–112.
589 doi:10.1134/S1063074020020042.
- 590 Elzhov, T.V., Mullen, K.M., Spiess, A.-N., and Bolker, B. 2023, September. Minpack.lm: R
591 Interface to the Levenberg-Marquardt Nonlinear Least-Squares Algorithm Found in MINPACK,
592 Plus Support for Bounds. [accessed 15 March 2024].

- 593 Falkowski, P.G., Katz, M.E., Knoll, A.H., Quigg, A., Raven, J.A., Schofield, O., and Taylor, F.J.R.
594 2004. The Evolution of Modern Eukaryotic Phytoplankton. *Science* **305**(5682): 354–360.
595 American Association for the Advancement of Science. doi:10.1126/science.1095964.
- 596 Falkowski, P., and Kolber, Z. 1993. Estimation of phytoplankton photosynthesis by active
597 fluorescence. *ICES Marine Science Symposium* **197**: 92–103.
- 598 Finkel, Z.V. 2001. Light absorption and size scaling of light-limited metabolism in marine
599 diatoms. *Limnology and Oceanography* **46**(1): 86–94. doi:10.4319/lo.2001.46.1.0086.
- 600 Flombaum, P., Gallegos, J.L., Gordillo, R.A., Rincón, J., Zabala, L.L., Jiao, N., Karl, D.M., Li,
601 W.K.W., Lomas, M.W., Veneziano, D., Vera, C.S., Vrugt, J.A., and Martiny, A.C. 2013. Present
602 and future global distributions of the marine Cyanobacteria *Prochlorococcus* and *Synechococcus*.
603 *Proceedings of the National Academy of Sciences* **110**(24): 9824–9829. *Proceedings of the*
604 *National Academy of Sciences*. doi:10.1073/pnas.1307701110.
- 605 Gorbunov, M.Y., Kuzminov, F.I., Fadeev, V.V., Kim, J.D., and Falkowski, P.G. 2011. A kinetic
606 model of non-photochemical quenching in cyanobacteria. *Biochimica et Biophysica Acta (BBA)*
607 *- Bioenergetics* **1807**(12): 1591–1599. doi:10.1016/j.bbabi.2011.08.009.
- 608 Grébert, T., Doré, H., Partensky, F., Farrant, G.K., Boss, E.S., Picheral, M., Guidi, L., Pesant, S.,
609 Scanlan, D.J., Wincker, P., Acinas, S.G., Kehoe, D.M., and Garczarek, L. 2018. Light color
610 acclimation is a key process in the global ocean distribution of *Synechococcus* cyanobacteria.
611 *Proceedings of the National Academy of Sciences* **115**(9): E2010–E2019. *Proceedings of the*
612 *National Academy of Sciences*. doi:10.1073/pnas.1717069115.

- Grossman, A.R., Mackey, K.R.M., and Bailey, S. 2010. A Perspective on Photosynthesis in the Oligotrophic Oceans: Hypotheses Concerning Alternate Routes of Electron Flow¹. *Journal of Phycology* **46**(4): 629–634. doi:10.1111/j.1529-8817.2010.00852.x.
- Guillard, R.R.L. 1975. Culture of phytoplankton for feeding marine invertebrates. *In* *Culture of Marine Invertebrate Animals: Proceedings — 1st Conference on Culture of Marine Invertebrate Animals Greenport. Edited by* W.L. Smith and M.H. Chanley. Springer US, Boston, MA. pp. 29–60. doi:10.1007/978-1-4615-8714-9_3.
- Hakala, M., Tuominen, I., Keränen, M., Tyystjärvi, T., and Tyystjärvi, E. 2005. Evidence for the role of the oxygen-evolving manganese complex in photoinhibition of Photosystem II. *Biochimica et Biophysica Acta (BBA) - Bioenergetics* **1706**(1): 68–80. doi:10.1016/j.bbabi.2004.09.001.
- Handel, A. 2020, October. Andreas Handel - Custom Word formatting using R Markdown. <https://www.andreashandel.com/posts/2020-10-07-custom-word-format/>. [accessed 13 June 2023].
- Harrison, W.G., and Platt, T. 1986. Photosynthesis-irradiance relationships in polar and temperate phytoplankton populations. *Polar biology* **5**: 153–164. Springer. [accessed 15 March 2024].
- Haverkamp, T.H.A. 2008. Shades of red and green : The colorful diversity and ecology of picocyanobacteria in the Baltic Sea. Yerseke Netherlands Institute of Ecology (NIOO) - Royal Netherlands Academy of Arts and Sciences. [accessed 3 July 2024].
- Haverkamp, T.H.A., Schouten, D., Doeleman, M., Wollenzien, U., Huisman, J., and Stal, L.J. 2009. Colorful microdiversity of *Synechococcus* strains (picocyanobacteria) isolated from the Baltic Sea. *The ISME Journal* **3**(4): 397–408. doi:10.1038/ismej.2008.118.

- 634 Hughes, D.J., Campbell, D.A., Doblin, M.A., Kromkamp, J.C., Lawrenz, E., Moore, C.M.,
635 Oxborough, K., Prášil, O., Ralph, P.J., Alvarez, M.F., and Suggett, D.J. 2018. Roadmaps and
636 Detours: Active Chlorophyll-a Assessments of Primary Productivity Across Marine and
637 Freshwater Systems. *Environmental Science & Technology* **52**(21): 12039–12054. American
638 Chemical Society. doi:10.1021/acs.est.8b03488.
- 639 Jávorfí, T., Erostyák, J., Gál, J., Buzády, A., Menczel, L., Garab, G., and Razi Naqvi, K. 2006.
640 Quantitative spectrophotometry using integrating cavities. *Journal of Photochemistry and*
641 *Photobiology B: Biology* **82**(2): 127–131. doi:10.1016/j.jphotobiol.2005.10.002.
- 642 Keeling, R.F., Körtzinger, A., and Gruber, N. 2010. Ocean Deoxygenation in a Warming World.
643 *Annual Review of Marine Science* **2**(Volume 2, 2010): 199–229. Annual Reviews.
644 doi:10.1146/annurev.marine.010908.163855.
- 645 Kirilovsky, D. 2015. Modulating energy arriving at photochemical reaction centers: Orange
646 carotenoid protein-related photoprotection and state transitions. *Photosynthesis Research* **126**(1):
647 3–17. doi:10.1007/s11120-014-0031-7.
- 648 Kolber, Z.S., Prášil, O., and Falkowski, P.G. 1998. Measurements of variable chlorophyll
649 fluorescence using fast repetition rate techniques: Defining methodology and experimental
650 protocols. *Biochimica et Biophysica Acta (BBA) - Bioenergetics* **1367**(1): 88–106.
651 doi:10.1016/S0005-2728(98)00135-2.
- 652 Larsson, J., Celepli, N., Ininbergs, K., Dupont, C.L., Yooseph, S., Bergman, B., and Ekman, M.
653 2014. Picocyanobacteria containing a novel pigment gene cluster dominate the brackish water
654 Baltic Sea. *The ISME Journal* **8**(9): 1892–1903. doi:10.1038/ismej.2014.35.

- 655 Latala, A., Jodłowska, S., and Pniewski, F. 2006. Culture Collection of Baltic Algae (CCBA) and
656 characteristic of some strains by factorial experiment approach. *Archiv fur Hydrobiologie* **122**:
657 137–154. [accessed 19 June 2024].
- 658 Llabrés, M., and Agustí, S. 2006. Picophytoplankton cell death induced by UV radiation: Evidence
659 for oceanic Atlantic communities. *Limnology and Oceanography* **51**(1): 21–29.
660 doi:10.4319/lo.2006.51.1.0021.
- 661 Llabrés, M., and Agustí, S. 2010. Effects of ultraviolet radiation on growth, cell death and the
662 standing stock of Antarctic phytoplankton. *Aquatic Microbial Ecology* **59**(2): 151–160.
663 doi:10.3354/ame01392.
- 664 Luimstra, V.M., Schuurmans, J.M., Verschoor, A.M., Hellingwerf, K.J., Huisman, J., and
665 Matthijs, H.C.P. 2018. Blue light reduces photosynthetic efficiency of cyanobacteria through an
666 imbalance between photosystems I and II. *Photosynthesis Research* **138**(2): 177–189.
667 doi:10.1007/s11120-018-0561-5.
- 668 Moore, L.R., Goericke, R., and Chisholm, S.W. 1995. Comparative physiology of *Synechococcus*
669 and *Prochlorococcus*: Influence of light and temperature on growth, pigments, fluorescence and
670 absorptive properties. *Marine Ecology Progress Series* **116**(1/3): 259–275. Inter-Research Science
671 Center. Available from <https://www.jstor.org/stable/44635011> [accessed 1 July 2024].
- 672 Morel, A. 1978. Available, usable, and stored radiant energy in relation to marine photosynthesis.
673 *Deep Sea Research* **25**(8): 673–688. doi:10.1016/0146-6291(78)90623-9.

- 674 Murphy, C.D., Roodvoets, M.S., Austen, E.J., Dolan, A., Barnett, A., and Campbell, D.A. 2017.
675 Photoinactivation of Photosystem II in *Prochlorococcus* and *Synechococcus*. *PLOS ONE* **12**(1):
676 e0168991. Public Library of Science. doi:10.1371/journal.pone.0168991.
- 677 Oxborough, K., and Baker, N.R. 1997. Resolving chlorophyll *a* fluorescence images of
678 photosynthetic efficiency into photochemical and non-photochemical components – calculation of
679 qP and F_v/F_m ; without measuring F_o ; *Photosynthesis Research* **54**(2): 135–142.
680 doi:10.1023/A:1005936823310.
- 681 Oxborough, K., Moore, C.M., Suggett, D.J., Lawson, T., Chan, H.G., and Geider, R.J. 2012. Direct
682 estimation of functional PSII reaction center concentration and PSII electron flux on a volume
683 basis: A new approach to the analysis of Fast Repetition Rate fluorometry (FRRf) data. *Limnology*
684 *and Oceanography: Methods* **10**(3): 142–154. doi:10.4319/lom.2012.10.142.
- 685 Partensky, F., Mella-Flores, D., Six, C., Garczarek, L., Czjzek, M., Marie, D., Kotabová, E.,
686 Felcmanová, K., and Prášil, O. 2018. Comparison of photosynthetic performances of marine
687 picocyanobacteria with different configurations of the oxygen-evolving complex. *Photosynthesis*
688 *Research* **138**(1): 57–71. doi:10.1007/s11120-018-0539-3.
- 689 Pedersen, T.L. 2024, January. Patchwork: The Composer of Plots. [accessed 20 April 2024].
- 690 Posit team. 2022. RStudio: Integrated development environment for r. Posit Software, PBC,
691 Boston, MA. Available from <http://www.posit.co/>.
- 692 R Core Team. 2023. R: A language and environment for statistical computing. R Foundation for
693 Statistical Computing, Vienna, Austria. Available from <https://www.R-project.org/>.

- 694 Scanlan, D.J. 2012. Marine Picocyanobacteria. *In* Ecology of Cyanobacteria II: Their Diversity in
695 Space and Time. *Edited by* B.A. Whitton. Springer Netherlands, Dordrecht. pp. 503–533.
696 doi:10.1007/978-94-007-3855-3_20.
- 697 Six, C., Finkel, Z.V., Irwin, A.J., and Campbell, D.A. 2007. Light variability illuminates niche-
698 partitioning among marine picocyanobacteria. PLOS ONE **2**(12): e1341. Public Library of
699 Science. doi:10.1371/journal.pone.0001341.
- 700 Śliwińska-Wilczewska, S., Cieszyńska, A., Maculewicz, J., and Latała, A. 2018a.
701 Ecophysiological characteristics of red, green, and brown strains of the Baltic picocyanobacterium
702 *Synechococcus* sp. – a laboratory study. Biogeosciences **15**(20): 6257–6276. Copernicus GmbH.
703 doi:10.5194/bg-15-6257-2018.
- 704 Śliwińska-Wilczewska, S., Maculewicz, J., Barreiro Felpeto, A., and Latała, A. 2018b.
705 Allelopathic and bloom-forming picocyanobacteria in a changing world. Toxins **10**(1): 48.
706 Multidisciplinary Digital Publishing Institute. doi:10.3390/toxins10010048.
- 707 Stomp, M., Huisman, J., de Jongh, F., Veraart, A.J., Gerla, D., Rijkeboer, M., Ibelings, B.W.,
708 Wollenzien, U.I.A., and Stal, L.J. 2004. Adaptive divergence in pigment composition promotes
709 phytoplankton biodiversity. Nature **432**(7013): 104–107. Nature Publishing Group.
710 doi:10.1038/nature03044.
- 711 Stomp, M., Huisman, J., Vörös, L., Pick, F.R., Laamanen, M., Haverkamp, T., and Stal, L.J. 2007.
712 Colourful coexistence of red and green picocyanobacteria in lakes and seas. Ecology Letters **10**(4):
713 290–298. doi:10.1111/j.1461-0248.2007.01026.x.

- 714 Strickland, J.D., and Parsons, T.R. 1972. Practical Hand Book of Seawater Analysis. Fisheries
715 Research Board of Canada **167 (2nd edition)**: 1–311. doi:DOI: [http://dx.doi.org/10.25607/OBP-](http://dx.doi.org/10.25607/OBP-1791)
716 1791.
- 717 Tortell, P., and Suggett, D.J. 2021. A user guide for the application of Single Turnover active
718 chlorophyll fluorescence for phytoplankton productivity measurements. Version 1. Report,
719 Scientific Committee on Oceanic Research (SCOR) Working Group 156. doi:10.25607/OBP-
720 1084.
- 721 Ulloa, O., Canfield, D.E., DeLong, E.F., Letelier, R.M., and Stewart, F.J. 2012. Microbial
722 oceanography of anoxic oxygen minimum zones. *Proceedings of the National Academy of*
723 *Sciences* **109**(40): 15996–16003. *Proceedings of the National Academy of Sciences*.
724 doi:10.1073/pnas.1205009109.
- 725 Ulloa, O., Henríquez-Castillo, C., Ramírez-Flandes, S., Plominsky, A.M., Murillo, A.A., Morgan-
726 Lang, C., Hallam, S.J., and Stepanauskas, R. 2021. The cyanobacterium *Prochlorococcus* has
727 divergent light-harvesting antennae and may have evolved in a low-oxygen ocean. *Proceedings of*
728 *the National Academy of Sciences* **118**(11): e2025638118. *Proceedings of the National Academy*
729 *of Sciences*. doi:10.1073/pnas.2025638118.
- 730 Wickham, H. 2016. Data Analysis. *In* *Ggplot2: Elegant Graphics for Data Analysis*. *Edited by* H.
731 Wickham. Springer International Publishing, Cham. pp. 189–201. doi:10.1007/978-3-319-24277-
732 4_9.
- 733 Wilson, A., Ajlani, G., Verbavatz, J.-M., Vass, I., Kerfeld, C.A., and Kirilovsky, D. 2006. A
734 Soluble Carotenoid Protein Involved in Phycobilisome-Related Energy Dissipation in
735 Cyanobacteria. *The Plant Cell* **18**(4): 992–1007. doi:10.1105/tpc.105.040121.

- 736 Włodkowiec, D., Czerw, A., Karakiewicz, B., and Deptała, A. 2022. Recent progress in cytometric
737 technologies and their applications in ecotoxicology and environmental risk assessment.
738 *Cytometry Part A* **101**(3): 203–219. doi:10.1002/cyto.a.24508.
- 739 Wong, J.C.Y., Raven, J.A., Aldunate, M., Silva, S., Gaitán-Espitia, J.D., Vargas, C.A., Ulloa, O.,
740 and von Dassow, P. 2023. Do phytoplankton require oxygen to survive? A hypothesis and model
741 synthesis from oxygen minimum zones. *Limnology and Oceanography* **68**(7): 1417–1437.
742 doi:10.1002/lno.12367.
- 743 Xu, K., Grant-Burt, J.L., Donaher, N., and Campbell, D.A. 2017. Connectivity among
744 Photosystem II centers in phytoplankters: Patterns and responses. *Biochimica et Biophysica Acta*
745 (BBA) - Bioenergetics **1858**(6): 459–474. doi:10.1016/j.bbabo.2017.03.003.
- 746 Xu, K., Lavaud, J., Perkins, R., Austen, E., Bonnanfant, M., and Campbell, D.A. 2018.
747 Phytoplankton σ_{PSII} and excitation dissipation; implications for estimates of primary
748 productivity. *Frontiers in Marine Science* **5**. doi:10.3389/fmars.2018.00281.

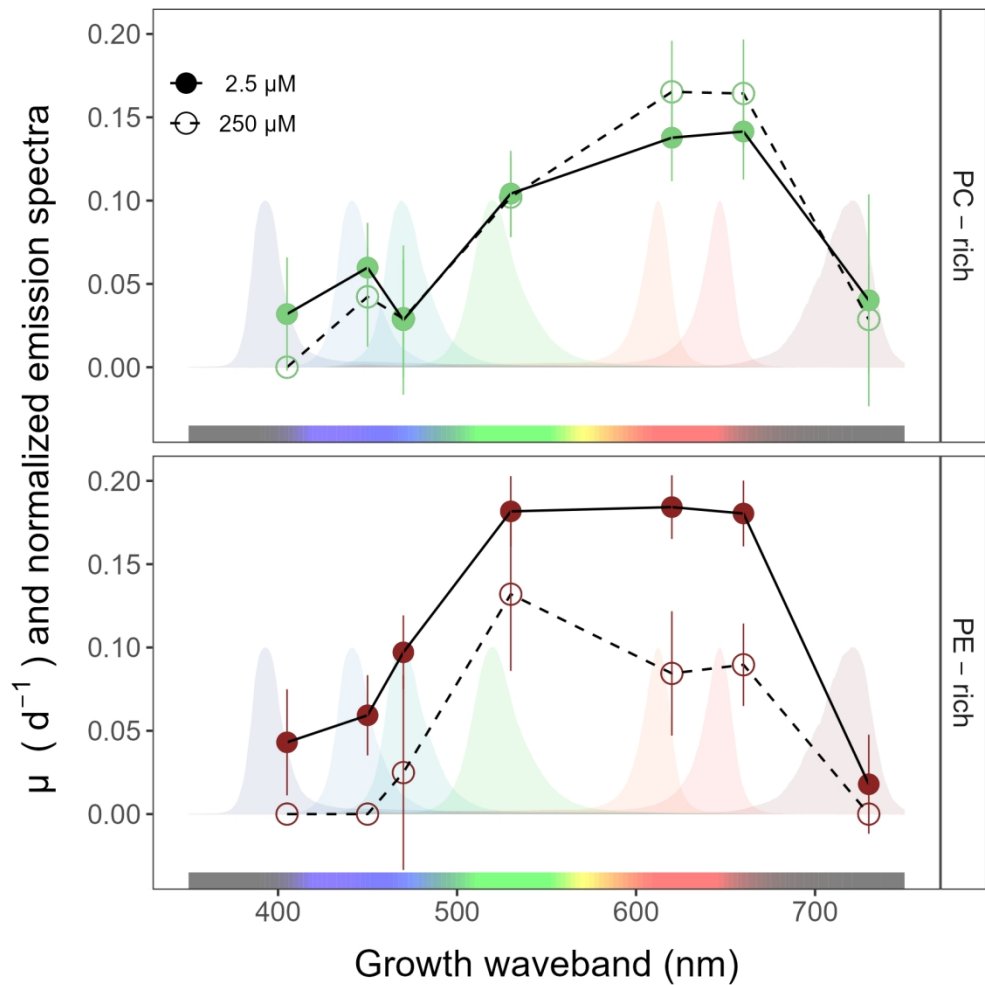


Fig. 1. Chlorophyll-specific growth rates (μ ; d⁻¹) vs. growth waveband (nm, shaded regions). Growth rates (\pm SE) were estimated from logistic fits of chlorophyll proxy OD680 – OD720 (Δ OD) vs. elapsed time (Fig. S1), for PC-rich (green circle) and PE-rich (red circle) cultures of *Synechococcus* grown at spectral wavebands of 405, 450, 470, 530, 620, 660, or 730 nm, and [O₂] of 250 μM (open symbols and dashed line) or 2.5 μM (closed symbols and solid line).

387x387mm (118 x 118 DPI)

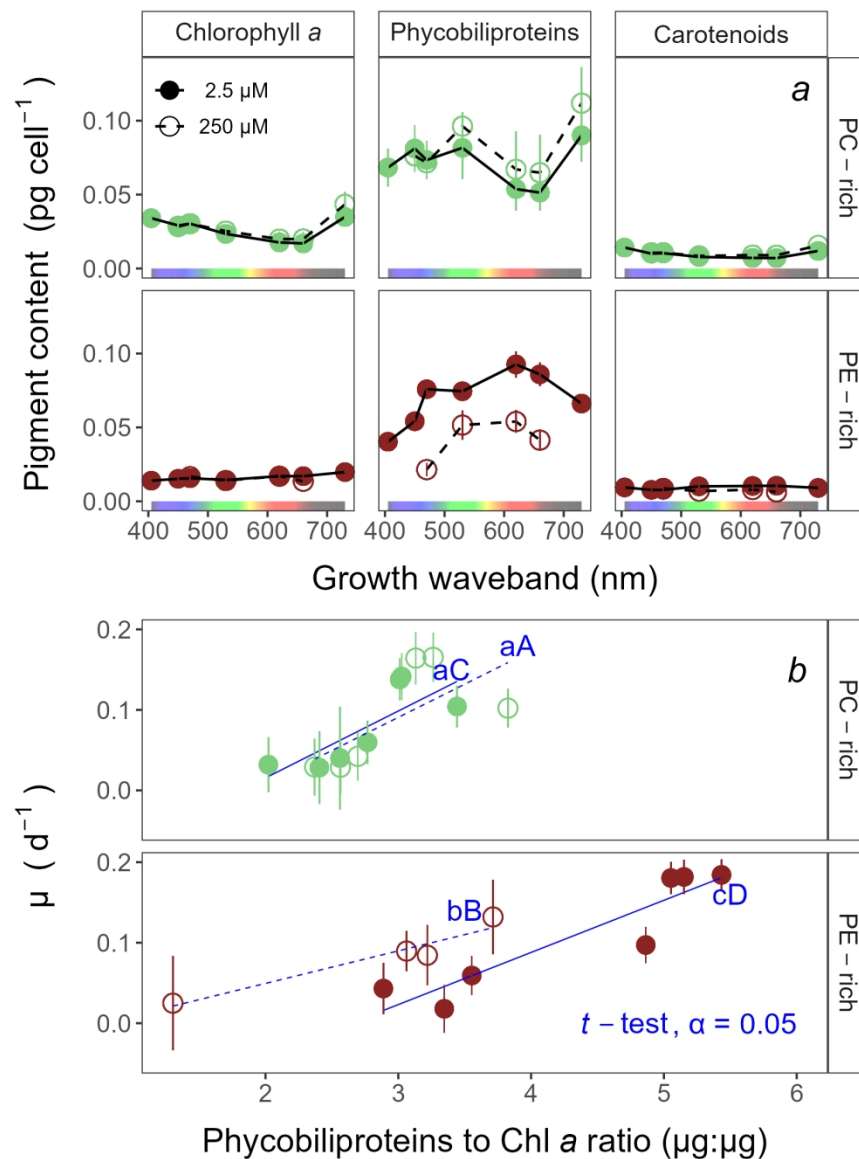


Fig. 2. Pigment content (pg cell⁻¹) vs. growth waveband (nm) (a) and Chlorophyll-specific growth rates (μ d⁻¹) vs. Phycobiliproteins:Chlorophyll a ratio (μg:μg) (b) for PC-rich (green circle) and PE-rich (red circle) cultures of *Synechococcus* grown at spectral wavebands of 405, 450, 470, 530, 620, 660, or 730 nm and 250 μM [O₂] (open symbols and dashed line) or 2.5 μM [O₂] (closed symbols and solid line). Data not presented for those PE-rich cultures which showed negligible growth under 405, 450, 730 nm and 250 μM [O₂]; nor for those PC-rich cultures which showed negligible growth under 405 nm and 250 μM [O₂]. Blue lines show linear model fit for data from each strain and [O₂] (solid for 2.5 μM [O₂] or dashed for 250 μM [O₂]) across spectral wavebands. Different blue lowercase letters indicate statistically significant differences between the fit models for different [O₂] within a given strain. Different blue uppercase letters indicate statistically significant differences between the fit models for different strains within a given [O₂] (t-test; p < 0.05).

387x516mm (118 x 118 DPI)

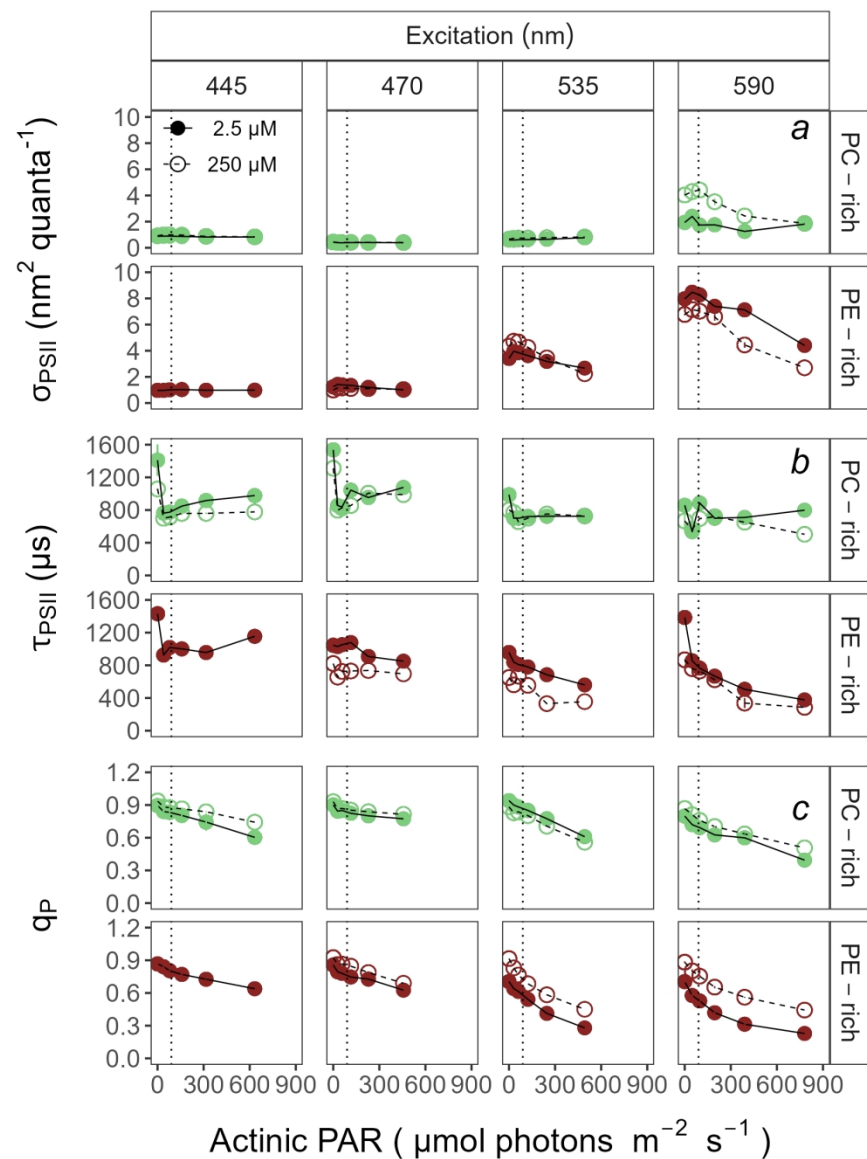


Fig. 3. Effective absorption cross section of PSII (σ_{PSII} ; nm² quanta⁻¹) (a); turnover time of PSII photochemistry (τ_{PSII} ; μs) (b); or photochemical quenching coefficient (q_p) (c) vs. Actinic PAR (μmol photons m⁻² s⁻¹). Parameters were estimated using FRRf induction curves with excitation (columns) at Ex445nm, blue; Ex470nm, blue-green; Ex535nm, green; or Ex590nm, orange; for PC-rich (green circle) or PE-rich (red circle) cultures of *Synechococcus*. Data show situations in which cultures were excited by, and growing in, corresponding growth wavebands of 450, 470, 530, or 620 nm and 250 μM [O₂] (open symbols and dashed line) or 2.5 μM [O₂] (closed symbols and solid line). The vertical lines show half diel peak PAR growth light of 90 μmol photons m⁻² s⁻¹. Data not presented for those PE-rich cultures which showed negligible growth under 405, 450, 730 nm and 250 μM [O₂]; nor for those PC-rich cultures which showed negligible growth under 405 nm and 250 μM [O₂].

387x516mm (118 x 118 DPI)

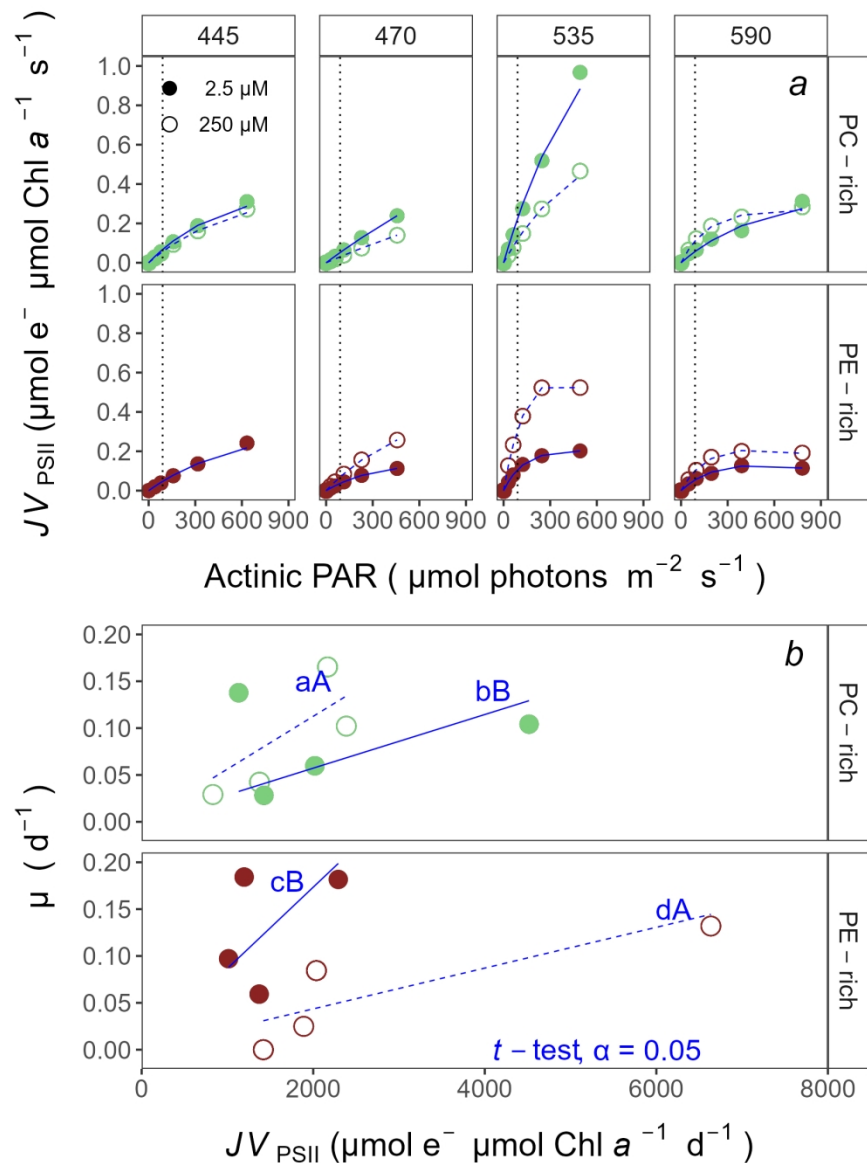


Fig. 4. PSII electron flux (JVPSII; $\mu\text{mol e}^- \mu\text{mol Chl a}^{-1} \text{s}^{-1}$) vs. Actinic PAR ($\mu\text{mol photons m}^{-2} \text{s}^{-1}$) (a). JVPSII was estimated using FRRf induction curves with excitation at Ex445nm, blue; Ex470nm, blue-green; Ex535nm, green; or Ex590nm, orange; for PC-rich (green circle) or PE-rich (red circle) cultures of *Synechococcus*. Data show situations in which cultures were excited by, and growing in, corresponding growth wavebands of 450, 470, 530, or 620 nm and 250 μM [O₂] (open symbols and dashed line) or 2.5 μM [O₂] (closed symbols and solid line). JVPSII vs. Actinic PAR ($\mu\text{mol photons m}^{-2} \text{s}^{-1}$) was fit with a Harrison and Platt Light Response Curve model (Harrison and Platt 1986), used to estimated JVPSII at 90 $\mu\text{mol photons m}^{-2} \text{s}^{-1}$ (vertical dotted lines). Chlorophyll-specific growth rates (μ ; d^{-1}) vs. PSII electron flux (JVPSII; $\mu\text{mol e}^- \mu\text{mol Chl a}^{-1} \text{d}^{-1}$) measured under half (90 $\mu\text{mol photons m}^{-2} \text{s}^{-1}$) of diel peak PAR growth light (b). Blue lines (solid for 2.5 μM [O₂] or dashed for 250 μM [O₂]) show linear model fit for data from each strain across spectral wavebands. Different blue lowercase letters indicate statistically significant differences between the fit models for different [O₂] within a given strain. Different blue uppercase letters indicate statistically significant differences between the fit models for different strains within a given [O₂] (t-test; $p < 0.05$).

387x516mm (118 x 118 DPI)